Source identification of nitrate in the upper aquifer system of the Wadi Shueib catchment area in Jordan based on stable isotope composition

Mutawakil OBEIDAT[1*], Muheeb AWAWDEH[2], Noor AL-KHARABSHEH[3], Ahmad AL-AJLOUNI[1]

[1] Faculty of Science and Arts, Jordan University of Science and Technology, Irbid 22110, Jordan;
[2] Laboratory of Applied Geoinformatics, Department of Earth and Environmental Sciences, Yarmouk University, Irbid 21163, Jordan;
[3] Department of Water Resources and Environmental Management, Al-Balqa Applied University, Al-Salt 19117, Jordan

Abstract: Groundwater forms the main freshwater supply in arid and semi-arid areas, and contamination of this precious resource is complicated by the slow rate of recharge in these areas. Nitrate contamination of groundwater is a global water quality problem, as it entails threat to human health as well as aquatic ecosystems. Source identification of contamination is the cornerstone and a prerequisite for any effective management program of water quality. Stable isotope composition of the dissolved nitrate (δ^{15}N-NO_3^- and δ^{18}O-NO_3^-) has been applied to identify NO_3^- sources and the main transformation processes in the upper aquifer system (A1/2, A4, and B2/A7 aquifers) in the Wadi Shueib catchment area, Jordan. Moreover, the stable isotope compositions of the groundwater (δ^2H-H_2O and $\delta 1^8$O-H_2O) in conjunction with the groundwater hydrochemistry were integrated to investigate the origin and evolution of the groundwater. Results revealed that groundwater in the study area is fresh and hard-very hard water, and mainly a Ca-Mg-Cl type. NO_3^- concentration was in the range of 7.0–74.0 mg/L with an average of 37.0 mg/L. Most of the samples showed concentration higher than the natural background concentration of NO_3^- (5.0–10.0 mg/L). The δ^2H-H_2O and δ^{18}O-H_2O values indicated that the groundwater is meteoric, and of Mediterranean origin, with a strong evaporation effect. The δ^{15}N-NO_3^- values ranged between 6.0‰ and 11.3‰ with an average of 8.7‰, and the δ^{18}O-NO_3^- values ranged between 1.6‰ and 5.9‰ with an average of 3.4‰. These values are in conformity with the stable isotope composition of nitrate derived the nitrification of wastewater/manure, and soil NH_4. Nitrification and denitrification are the main transformation processes affecting nitrogen species. Statistical analysis revealed no significant differences in the δ^2H-H_2O and δ^{18}O-H_2O values, and δ^{15}N-NO_3^- and δ^{18}O-NO_3^- values for the three aquifers (A1/2, A4, and B2/A7), indicating that the groundwater of these aquifers has the same origin, and a common source of pollution.

Keywords: δ^{15}N-NO_3^-; δ^{18}O-NO_3^-; nitrate sources; pollution; meteoric origin; aquifer; Jordan

1 Introduction

Similar to arid and semi-arid areas, groundwater represents the main supply of freshwater in Jordan. However, it has been contaminated and depleted due to excessive pumping. The Sustainable

*Corresponding author: Mutawakil OBEIDAT (E-mail: mobeidat@just.edu.jo)
Received 2020-02-23; revised 2020-05-14; accepted 2020-06-21

Development Goals (SDGs) of the United Nations Development Program (UNDP) classified the sustainable management and protection of groundwater as a top priority (Megdal et al., 2017; Senarathne et al., 2019). Groundwater contamination by nitrate is a common environmental problem worldwide (Popescu et al., 2015; Soldatova et al., 2017; Machiwal et al., 2018). It is a challenging problem due to the slow rate of recharge, particularly in arid and semi-arid areas where groundwater represents the main source of freshwater for domestic and agricultural uses (Re et al., 2017; Gutierrez et al., 2018). Natural background concentration of nitrate in groundwater is in the range of 5.0–10.0 mg/L as NO_3^- (Panno et al., 2006). Water contamination by nitrate has ecological effects such as eutrophication, oxygen depletion, and anoxia as well as threats to human health, such as methemoglobinemia and stomach cancer (Kendall et al., 2007; Nixon, 2009; Kaushal et al., 2011; WHO, 2011; Jankowski et al., 2012; Chen et al., 2013; Lehmann et al., 2015; Yang et al., 2016). The maximum permissible limits in groundwater set by national and international organizations (such as WHO; 50.0 mg/L as NO_3^-) have been reported worldwide (e.g., Choi et al., 2000; Obeidat et al., 2007; Obeidat et al., 2012; Karroum et al., 2017; Re and Sacchi, 2017; Nejatijahromi et al., 2019; Tarawneh et al., 2019). Elevated nitrate concentration in the Wadi Shueib of Jordan has been reported by several studies. Al-Kharabsheh and Al-Kharabsheh (2014) reported nitrate concentration in ten springs in the Wadi Shueib to be in the range of 27.0–104.0 mg/L. Nitrate concentration in the range of 23.0–86.0 mg/L in five springs emerging in the Wadi Shueib was found by Grimmeisen et al. (2017). Nitrate concentration of more than 110.0 mg/L was reported for some springs in the Wadi Shueib (Margane et al., 2010). Nitrate concentration in the range of 21.0–66.0 mg/L in 11 springs and 3 wells in the Wadi Shueib was found by Awawdeh et al. (2020). Nitrate in groundwater has been commonly linked to agricultural fertilizers (Wakida and Lerner, 2005). However, non-agricultural sources such as wastewater disposal and landfills are important sources of nitrate in groundwater (Gold et al., 1990; Jeon, 2001; Huang et al., 2013; Zhang et al., 2015; Kapelewska et al., 2019; Tiwari et al., 2019; Zendehbad et al., 2019; Obeidat et al., 2020; Yu et al., 2020).

Source identification of nitrate and transformation processes of nitrogen species in water is fundamental in any management program of water resources and water pollution control (Johannsen et al., 2008; Hoefs, 2009; Popescu et al., 2015). Several approaches have been developed to trace water pollution. These include solute transport modelling, statistical modelling and chemical fingerprinting approaches (e.g., Mattern et al., 2009; Qin et al., 2013; Shalev et al., 2015; Levy et al., 2017; Aravinthasamy et al., 2019; Bodrud-Doza et al., 2019; Rashid et al., 2019; Guo et al., 2020; Huan et al., 2020; Jia et al., 2020; Lee et al., 2020; Nyam et al., 2020). In the context of the latter approach, nitrate sources can be investigated using the following methods (Zendehbad et al., 2019): the isotope composition of groundwater and dissolved nitrate, the chemistry and isotope composition of major and trace elements in groundwater, the pollutants of known origins found in association with nitrate, and the groundwater age. Boron (B) isotopes have been used in conjunction with nitrogen isotopes to identify nitrate sources in groundwater, as these elements co-migrate in the aquifer, where B is unaffected by the redox reaction and biologic transformation that affect nitrogen compounds (Martinelli et al., 2018; Kruk et al., 2020). The $\delta^{11}B$ values can be used to distinguish manure form sewage sources of nitrate in groundwater (Biddau et al., 2019). Strontium (Sr) ratio ($^{87}Sr/^{86}Sr$) has also been utilized to better identify the nitrate sources in groundwater, because its isotopic composition, as a result of water-rock interaction, is distinct from that of anthropogenic origin (Nigro et al., 2017). Integration of water chemistry with isotope composition of the dissolved nitrate ($\delta^{15}N\text{-}NO_3^-$ and $\delta^{18}O\text{-}NO_3^-$), sulfate ($\delta^{34}S\text{-}SO_4^{2-}$ and $\delta^{18}O\text{-}SO_4^{2-}$), and $\delta^{13}C$ of dissolved carbon has been used to investigate denitrification process and the factors that control it (Vitoria et al., 2008; Kaown et al., 2009). Moreover, groundwater age has been used as an indicator of direct migration of pollutants derived from the earth surface; tracers such as chlorofluorocarbon (CFC), tritium, and ^{14}C have also been utilized (Tesoriero et al., 2007; Koh et al., 2010; Jakobczyk-Karpierz et al., 2017). Meanwhile, a multi-isotopic approach in conjunction with the groundwater hydrochemistry, and statistical modelling such as principal component analysis have been applied to track nitrate and pollution sources in groundwater (Vitoria et al., 2008; Guo et al., 2020; Zhang and Wang, 2020).

In the last decades, nitrogen and oxygen isotopes of the dissolved nitrate ($\delta^{15}N\text{-}NO_3^-$ and $\delta^{18}O\text{-}NO_3^-$) have been successfully applied to tackle nitrate contamination of groundwater (Czekaj et al., 2016; Hu et al., 2019; Venkiteswaran et al., 2019; Zhao et al., 2019; Kruk et al., 2020; Li et al., 2020; Sui et al., 2020). Combining $\delta^{15}N\text{-}NO_3^-$ with $\delta^{18}O\text{-}NO_3^-$ results can help to identify nitrate sources, mixing processes, and transformation processes of nitrate (Kendall et al., 2007; Xue et al., 2009; Thibodeau et al., 2013; Archana et al., 2018). Different sources of nitrate have distinct isotopic composition of $\delta^{15}N\text{-}NO_3^-$ and $\delta^{18}O\text{-}NO_3^-$ (Widory et al., 2013). $\delta^{15}N\text{-}NO_3^-$ values of atmospheric nitrate, nitrate resulting from the nitrification of manure or sewage, nitrate in synthetic fertilizer, and natural soil organic matter are in the ranges from –13.0‰ to 13.0‰, 7.0‰ to more than 20.0‰, –3.0‰ to 3.0‰, and –3.0‰ to 5.0‰, respectively (Mayer et al., 2002; Lee et al., 2008; Xue et al., 2009; Gutierrez et al., 2018). On the other hand, $\delta^{18}O\text{-}NO_3^-$ values of atmospheric nitrate, nitrate in synthetic fertilizer, and nitrification-derived nitrate are in the ranges from 25.0‰ to more than 70.0‰, 17.0‰ to 25.0‰, and –15.0‰ to 15.0‰, respectively (Durka et al., 1994; Mayer et al., 2002; Kendall et al., 2007; Xue et al., 2009). Moreover, the contributions of different sources can be estimated using isotope mass-balance mixing models, which are based on $\delta^{15}N\text{-}NO_3^-$ and $\delta^{18}O\text{-}NO_3^-$ values (Moore et al., 2006; Parnell et al., 2010; Zhang et al., 2015; Matiatos, 2016; Xia et al., 2017; Zhang et al., 2018).

The stable isotope composition of the dissolved nitrate ($\delta^{15}N\text{-}NO_3^-$ and $\delta^{18}O\text{-}NO_3^-$) is subject to modification by isotopic fractionation caused by physical, chemical, and biological processes, such as volatilization, assimilation, nitrification, and denitrification (Kaown et al., 2010). Nitrification is a two-step process of NH_4^+ oxidation to NO_3^- (Kendall et al., 2007; Gutierrez et al., 2018): the first step is called nitritation, where ammonia-oxidizing bacteria decompose organic nitrogen and ammonium under aerobic condition into nitrite; the second step is called nitratation, where nitrite-oxidizing bacteria convert nitrite to nitrate. Nitrate originating from oxidation of animal waste/septic waste has a high $\delta^{15}N$ value due to volatilization of $\delta^{15}N$ depleted ammonia, and subsequent oxidation of much of the residual waste material (Kendall et al., 2007). For animal waste with a $\delta^{15}N$ value of around 5.0‰, the $\delta^{15}N$ values are generally in the range of 10.0‰–20.0‰ when it is transformed to nitrate (Kreitler, 1979). Denitrification converts nitrate to N_2 gas; it is a significant transformation process, since it plays a vital role in attenuating nitrate concentrations. It occurs under the following conditions (Gutierrez et al., 2018): (1) oxygen concentration less than 1.0–2.0 mg/L (occur in anaerobic pockets within an otherwise oxygenated sediment or water body); (2) presence of denitrifying bacteria, nitrate, and electron donor; (3) temperature of 25°C–35°C; (4) pH values of 5.5–8.0; and (5) trace nutrients.

In some situations, the isotopic composition of nitrate overlaps among the different source materials and/or between source signatures and process signals (Chang et al., 2003). To overcome this drawback, the integration of hydrochemical tools with the isotope approach is very helpful (Widory et al., 2013). Researches worldwide showed that the combination of nitrate isotopes ($\delta^{15}N\text{-}NO_3^-$ and $\delta^{18}O\text{-}NO_3^-$) with other tools such as hydrochemistry, statistical methods, and physical and chemical modeling give useful insights about nitrate sources and transformation processes of nitrogen in the environment (Clague et al., 2015; Soldatova et al., 2017; Biddau et al., 2019). Conventional hydrochemical methods have been successfully used to characterize water type, and evaluate the processes controlling the water chemistry and degradation of aquifers (Abu-alnaeem et al., 2018; Tiwari et al., 2019). Schoeller indices (such as chloro-alkaline index, CAI) have been used to get insights about ion exchange reactions between groundwater and the hosting aquifer material, as well as information about freshening or salinizing processes of groundwater (Stuyfzand, 2008; Abu-alnaeem et al., 2018; Tiwari et al., 2019). The CAI can be determined using the following equation (Schoeller, 1967):

$$CAI = (Cl^- - (Na^+ + K^+)) / Cl^-, \quad (1)$$

where Cl^- is the chloride concentration (meq/L); Na^+ is the sodium concentration (meq/L); and K^+ is the potassium concentration (meq/L).

CAI values could be negative or positive depending on whether the exchange of Na^+ and K^+ is from water with Mg^{2+} and Ca^{2+} in rock/soil or vice versa (Tiwari et al., 2019). There are two types

of ion exchange processes (Ayadi et al., 2018): the first one is known as reverse ion exchange process, where Na^+ and K^+ are sequestered onto the aquifer material, and Ca^{2+} and Mg^{2+} are released into the water. The CAI values in this case are positive, and there is hardening of water (Zaidi et al., 2015). The second type is known as base ion exchange process, where Ca^{2+} and Mg^{2+} are sequestered onto the aquifer material and Na^+ and K^+ are released into the water. The CAI values in this case are negative, and there is softening of water (Argamasilla et al., 2017).

Tackling and understanding natural as well as anthropogenic processes/factors influencing the groundwater quality and its evolution is very crucial for the protection and sustainability of this priceless resource. This study aims at tracing sources and transformation of nitrogen species in a three-aquifer system, which includes Na'ur aquifer (A1/2), Hummar aquifer (A4), and Amman/Wadi Wadi Es Sir aquifer (B2/A7) in the Wadi Shueib catchment area using hydrochemical methods, and stable isotopes of groundwater (δ^2H and $\delta^{18}O$) and dissolved nitrate ($\delta^{15}N\text{-}NO_3^-$ and $\delta^{18}O\text{-}NO_3^-$). The results of this study can help initiating prevention/remediation measures of groundwater contamination in the Wadi Shueib catchment area.

2 Materials and methods

2.1 Study area

The study area (31°53′01″–32°05′10″N, 35°37′32″–35°50′29″E) is located at the western slopes of the eastern highlands of the Jordan rift valley and it covers an area of 200 km^2 (Fig. 1a). It has a rectangular shape, with the long axis being oriented from northeast to southwest. Elevations range from 181 m below sea level (b.s.l.) in the southwest to 1136 m above sea level (a.s.l.) in the northeast. Several Wadis are found in the catchment area that are all draining from northeast to southwest toward the Jordan valley. The study area is generally dominated by the Mediterranean climate, which is characterized by hot summers and cold winters. Due to the strong relief, the climatic conditions considerably vary from the arid Jordan valley to the Mediterranean climate in the highlands in the northeast. Precipitation occurs periodically during the rainy season between October and May and it is normally associated with frontal systems moving inland from the Mediterranean Sea (Margane et al., 2010). The average annual precipitation is highly variable over the basin, and it is influenced by the topography (Riepl, 2013). Precipitation is 599 mm for Hummar station (953 m a.s.l.), which is located 3.5 km northeast of Fuheis City, and 175 mm for South Shuna station (143 m b.s.l.), which is located in the eastern edge of South Shuna City. The annual average temperatures vary between 17.3°C in Salt station and 25.6°C in South Shuna station (Fig. 1b).

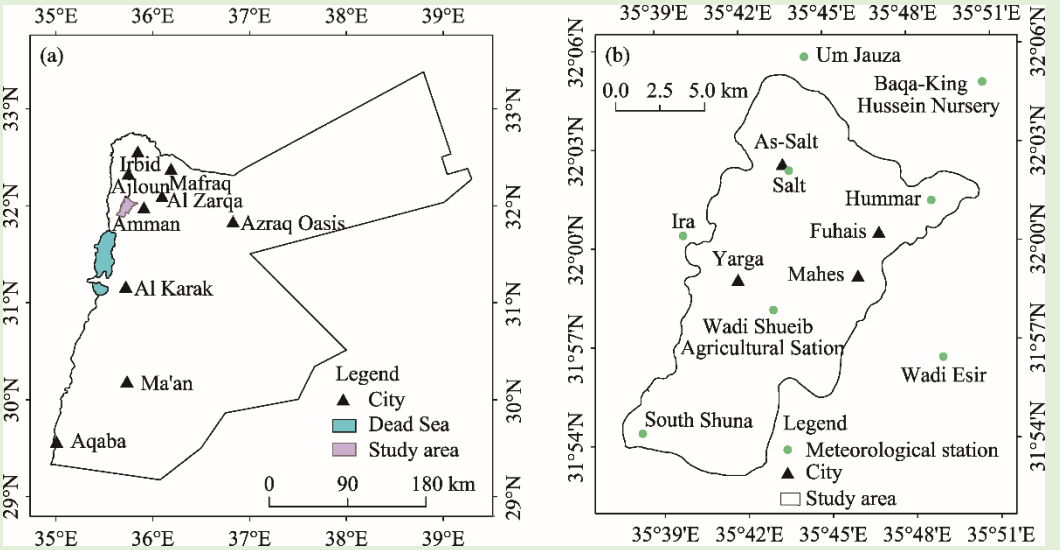

Fig. 1 Location of the study area in Jordan (a) and distribution of the meteorological stations in the study area (b)

The geology of the investigated area is dominated by the sedimentary rocks of the Upper Cretaceous, which consists mainly of limestone, dolomite, and marls of the Ajloun (A) and Belqa (B) groups (Fig. 2). These are underlain by sandstones of the Kurnub group of the Lower Cretaceous age, outcropping on fault zones along Wadi Shueib structure (Mikbel and Zacher, 1981). The Kurnub Sandstone consists mainly of cross-bedded massive bodies of porous varicolored quartz arenite, and glauconitic sandstone. Particle size is coarse to medium sand fraction, usually loosely cemented (Kuntz, 2003). In the upper layers, carbonate cementation is evident and particle size becomes finer. The thickness of the Kurnub Sandstone is approximate 250 m (Powell, 1989). The A and B groups are divided into a number of formations, ranging from A1 to A7 for the former, and from B1 to B5 for the latter (Masri, 1963). The A group consists of approximately 350–400 m thick interbedded limestones, marly limestones, and dolomitic limestones, whereas the B group mainly includes a sequence of limestones, intercalated with thick-bedded chert but also includes chalk, marls, silicified limestones, and phosphatic horizons (Werz, 2006).

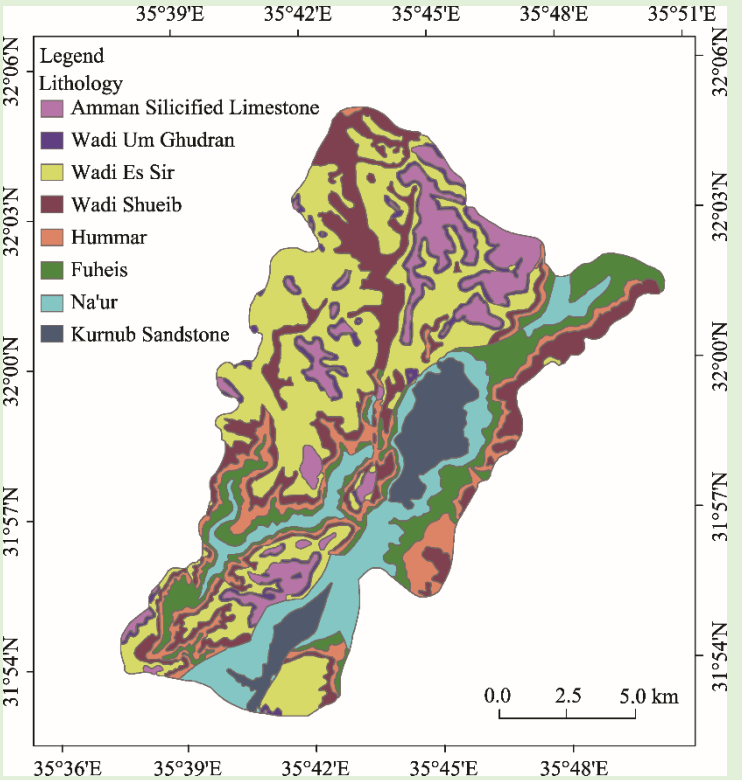

Fig. 2 Geological map of the study area

Na'ur formation (A1/2) of Cenomanian age overlies the Kurnub Sandstone formation, where two units are distinguished within this formation. First, a lower formation (A1) consists mainly of marls with a thickness of 37–80 m. Second, an upper formation (A2) consists mainly of limestone and marly limestone, with a thickness of 74–100 m. Fuheis formation (A3) of Cenomanian age is overlying Na'ur formation, and mainly consists of marl and interbedded limestone with a thickness of 69–75 m. Hummar formation (A4) of Cenomanian age consists of hard dense limestone and dolomitic limestone. Wadi Shueib formation (A5/6) of the upper Turonian age is composed mainly of marly limestone and chalky marl. This formation has a thickness of 50–80 m, and is divided into two sub-formations (Masri, 1963; MacDonald, 1965): A5, which is composed of thinly-bedded buff to grey limestone with thin marl intercalations; and A6, which is composed of white to grey crystalline massively bedded limestone. Wadi Es Sir formation (A7) of Turonian age consists of light grey, hard limestone with chert nodules. It has a thickness of 75–150 m. The B group overlies the A group with a sequence of predominantly carbonates with abundant chert. It has been

subdivided into five formations (B1–B5); only two of these are found in the study area, namely Wadi Um Ghudran formation (B1) and Amman Silicified Limestone formation (B2). The former is of Santonian age and is composed of well-bedded chalk and marl, with occasional beds of limestone with a thickness of 15 m (Ta'any, 1992); the latter is of Campanian age and consists of chert, marl, limestone, and some phosphatic bearing strata, with a total thickness of about 20 m. In some places, B1 is missing, and thus B2 directly overlies A7, forming a composite aquifer (B2/A7).

From a hydrogeological point of view, the aquifer systems are divided into two main aquifer systems (GTZ, 1977): the lower Cretaceous complex (Kurnub Sandstone), and the upper Cretaceous aquifer complex. This classification is based on lithology and hydrogeological conditions. The lower aquifer system, exposed in the west of Mahis Town, consists of varicolored sandstone with a thickness of 220–300 m; it is separated from the upper complex by a low permeability layer of 2×10^{-8} m/s (Geyh et al., 1986). The upper aquifer system includes the A and B groups with an age ranging from upper Cretaceous to lower Tertiary. A group represents the main aquifer system in the study area, where the aquifers are composed of limestone, dolomitic limestone, and marl. Three main formations of this group are considered aquifers. These are Na'ur formation (A1/2), Hummar formation (A4), and Wadi Es Sir formation (A7). On the other hand, Wadi Shueib and Fuheis formations are classified as aquitards. The whole aquifer is an unconfined system. There are 22 springs emerging from this aquifer system: five from A4, nine from A7, and eight from A1/2 (Al-Kharabsheh and Al-Kharabsheh, 2014). The Fuheis and Wadi Shueib formations are strongly vertically jointed and fractured causing the whole upper aquifer system to be hydraulically interconnected through joints and fault zones (Werz, 2006). There are only two formations from the B group which are exposed in the study area: Wadi Um Ghudran formation (B1) and Amman formation (B2), where B1 is classified as aquitard and B2 as aquifer (Werz, 2006). Because of insufficient wells in the study area, a groundwater level map cannot be constructed. However, Werz (2006) estimated the average depth of the groundwater as follows: 50 m for the Hummar aquifer (A4), 60 m for the Na'ur aquifer (A1/2), and 75 m the for Wadi Es Sir aquifer (A7). According to Zemann et al. (2015), the groundwater flow direction is towards southwest. Direct recharge from precipitation was estimated at 21% (9.9×10^6 m^3) of the annual precipitation (WSPSP, 2004). The main hydraulic properties of the aquifer system are summarized in Table 1 (Margane et al., 2009). Water needs in the study area are covered from the local groundwater (50%), and water imported from King Abullah Canal (50%). The water supplied for domestic purposes is about 5.4×10^6 m^3/a. The basin is dominated by four main land covers (Fig. 3): rainfed cropland (40.72%), built-up areas (17.80%), barren areas (15.10%), and sparse vegetation (14.73%). The study area hosts two wastewater treatment plants: Salt Wastewater Treatment Plant and Fuheis Wastewater Treatment Plant, which release their effluents into the main Wadi Shueib stream (Grimmeisen et al., 2017). Leaky sewers and cesspits are the main sources of contamination of the groundwater in the study area (Margane et al., 2010).

Table 1 Hydraulic properties of the hydrogeological system in the study area (Margane et al., 2009)

Hydrogeological unit	Aquifer potentiality	Thickness (m)	Hydraulic conductivity (m/d)
B2/A7	Aquifer	140–265	2
A5/6	Aquitard	50–60	1×10^{-4}
A4	Aquifer	40–65	2
A3	Aquitard	50–80	1×10^{-4}
A1/2	Aquifer	86–200	1
Kurnub	Aquifer	150–50	3

Note: B2, Amman formation; A7, Wadi Es Sir formation; B2/A7, composite aquifer of B2 and A7; A5/6, Wadi Shueib Formation; A4, Hummar formation; A3, Fuheis formation; A1/2, Na'ur formation; Kurnub, Kurnub Sandstone formation.

2.2 Experimental design and data collection

Seventeen samples were collected from the upper aquifer system in the study area representing 11 springs and 6 production wells (Fig. 3). Seven samples were collected from the B2/A7 (six springs

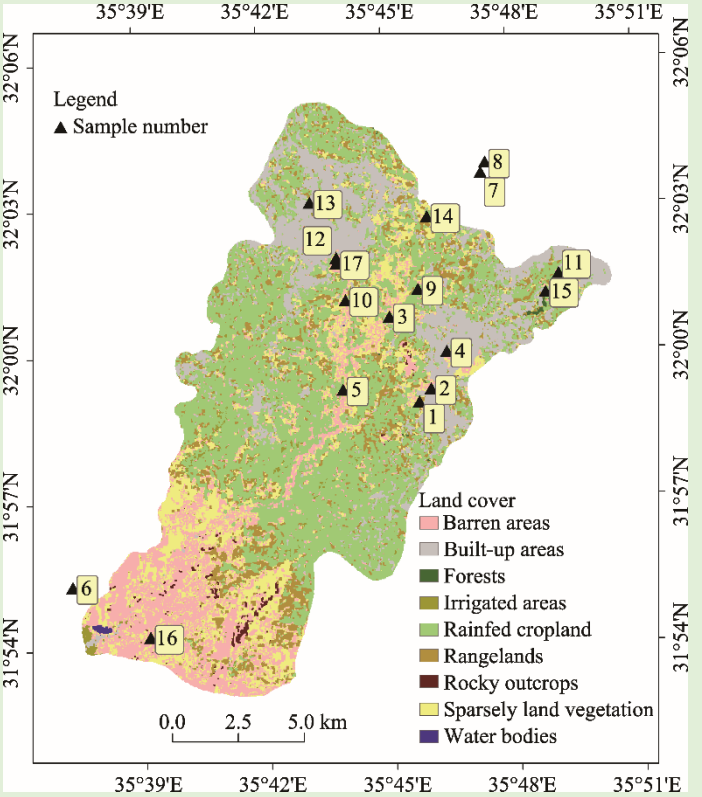

Fig. 3 Distribution of the land cover in the study area (Jawarneh and Biradar, 2017). Sample locations are also shown.

and one production well), seven samples from the A4 aquifer (three springs and four production wells), and three samples from the A1/2 aquifer (two springs and one production well). The sampling campaign was conducted in the rainy season in January and February of 2018. The sampled wells are production wells used to supply local community with freshwater. The sampled wells (samples 8, 13, 14, and 16) for tapping the A4 aquifer have a depth varying from 166 to 285 m. The sampled well (sample 6) which taps the A1/2 aquifer has a depth of 377 m, and that well (sample 7) which taps the B2/A7 aquifer has a depth of 283 m. All water samples were field pre-filtered through 0.45 μm Millipore filters into HDPE (high-density polyethylene) sample bottles with appropriate storage and preservation methods (e.g., refrigeration, freezing, acidification, and addition of chloroform). The methods described by APHA (1998) were followed during fieldwork and laboratory chemical analyses. Electrical conductivity (EC), temperature, and pH were measured *in situ* using portable meters. Prior to sample collection, well purging was performed for those wells, which were not being pumped at the time of sampling. The goal was to ensure that the water sample truly represents the properties and conditions of the subsurface environment. Water was pumped from each well until the EC, temperature, and pH became constant. Spring samples, on the other hand, were sampled at the mouth of springs.

Chemical analyses were carried out in the laboratories of Jordan University of Science and Technology and Yarmouk University, Jordan. The samples were analyzed for Ca^{2+}, Mg^{2+}, Na^{+}, K^{+}, Cl^{-}, HCO_3^{-}, SO_4^{2-}, NO_3^{-}, total hardness (TH), and total dissolved solids (TDS). Concentrations of Ca^{2+}, Mg^{2+}, Na^{+}, K^{+}, Cl^{-}, and SO_4^{2-} were analyzed using the Thermo Scientific Ion Chromatograph (Dionix ICS-1600, ThermoFisher Scientific, Waltham, USA). HCO_3^{-} and NO_3^{-} concentrations were determined by titration method and spectrophotometer, respectively. All samples were analyzed in triplicate with analytical uncertainty of less than 4%. We used the cations–anions balance to check the correctness of the analysis, where it was within ±5%, which was calculated as follows:

$$\text{Error (\%)} = \left| \frac{\sum \text{Cations} - \sum \text{Anions}}{\sum \text{Cations} + \sum \text{Anions}} \right| \times 100\%. \quad (2)$$

This value guarantees the reliability of the chemical analysis. TDS content (mg/L) was determined using a conductivity meter (HACH portable EC meter, HACH, Colorado, USA). TH value (mg/L) was calculated using the following equation:

$$\text{TH as } CaCO_3 = 2.5Ca + 4.1Mg, \quad (3)$$

where $CaCO_3$, Ca, and Mg are the concentrations (mg/L) of $CaCO_3$, Ca^{2+}, and Mg^{2+}, respectively.

The importance of the saturation index (SI) is to determine the dissolution or precipitation during the water–rock interaction. The SI of a mineral can be calculated using the equation as follows:

$$SI = \log\left(K_{IAP} / K_{SP}\right), \quad (4)$$

where SI is the saturation index; K_{IAP} is the ionic activity product of the appropriate ion; and K_{SP} is the solubility product of the mineral. If the SI=0, it means that the water is in equilibrium. If the SI>0, it means that the water is supersaturated with respect to that mineral, and the mineral is precipitated. If the SI<0, it means that the water is undersaturated with respect to the mineral, and the dissolution process is taking place.

The saturation indices of the minerals calcite, dolomite, halite, and gypsum were calculated using the computer program PHREEQC (version 3.3.7.11094, USGS, USA) (Parkhurst and Appelo, 1999).

The $\delta^{15}N\text{-}NO_3^-$, $\delta^{18}O\text{-}NO_3^-$, $\delta^{18}O\text{-}H_2O$, and $\delta^{2}H\text{-}H_2O$ values were determined at the Environmental Isotope Laboratory, University of Waterloo, Canada, by using the cadmium reduction method (Mcilvin and Altabet, 2005) to convert NO_3^- to N_2O and were coupled with a Trace Gas-GVI IsoPrime-IRMS (TG-IRMS). The analytical precision of the laboratory analysis is ±0.3 and ±0.8 for $\delta^{15}N\text{-}NO_3^-$ and $\delta^{18}O\text{-}NO_3^-$, respectively. The $^2H/^1H$ and $^{18}O/^{16}O$ ratios of the water samples were measured using a Los Gatos Research (LGR), a Liquid Water Isotope Analyzer (LWIA), and a model T-LWIA-45-EP instrument (Los Gatos Research, Mountain View, California), with an analytical precision of ±0.2 and ±0.8 for $\delta^{2}H\text{-}H_2O$ and $\delta^{18}O\text{-}H_2O$, respectively. The stable isotope ratio (δ_{sample}; ‰) was calculated as followings:

$$\delta_{sample}\ (‰) = \left[\left(R_{sample} - R_{standard}\right) / R_{standard}\right] \times 1000‰, \quad (5)$$

where R_{sample} and $R_{standard}$ are the $^{15}N/^{14}N$, $^2H/^1H$, or $^{18}O/^{16}O$ ratios of the sample and international reference standard, respectively. Values of $\delta^{15}N$ were reported relative to N_2 in atmospheric air, and $\delta^{18}O$ and $\delta^{2}H$ values were reported relative to Vienna Standard Mean Ocean Water (VSMOW). Isotopic data of precipitation in Jordan were obtained from the Water Authority of Jordan (WAJ).

2.3 Statistical analysis

Statistical analyses, including univariate and bivariate statistics, and one-way analysis of variance (ANOVA) test were performed using the software package SPSS 13 (version 21, SPSS Inc., Chicago, II, USA). The one-way ANOVA test was used to test if there were significant differences in the isotope composition of the groundwater ($\delta^{2}H\text{-}H_2O$ and $\delta^{18}O\text{-}H_2O$ values), and nitrate isotopes ($\delta^{15}N\text{-}NO_3^-$ and $\delta^{18}O\text{-}NO_3^-$ values) for the three aquifers (A1/2, A4, and B2/A7). The *P*-value≤0.05 was used as the criterion for statistical difference.

3 Results and discussion

3.1 Major ion chemistry

The univariate statistics of the hydrochemical parameters of the groundwater samples representing the whole aquifer complex in the study area are shown in Table 2. The following is a brief discussion of the major ion chemistry of individual aquifer units.

3.1.1 Na'ur aquifer (A1/2)

Three water samples, one from production wells (sample 6) and two from springs (samples 1 and

Table 2 Descriptive statistics of the hydrochemical parameters of the groundwater samples

Parameter	Minimum	Maximum	Mean	Maximum permissible concentration recommended by WHO (2011)	Standard deviation	Coefficient of variation (%)
NO_3^- (mg/L)	7.1	74.4	37.0	50.0	18.0	47
Cl^- (mg/L)	33.0	156.0	87.0	600.0	38.0	43
SO_4^{2-} (mg/L)	22.0	118.0	51.0	600.0	29.0	57
HCO_3^- (mg/L)	104.0	180.0	158.0	600.0	17.0	11
Na^+ (mg/L)	22.0	81.0	47.0	200.0	22.0	46
K^+ (mg/L)	1.0	14.0	4.0	200.0	4.0	107
Mg^{2+} (mg/L)	12.0	40.0	24.0	500.0	7.0	31
Ca^{2+} (mg/L)	62.0	137.0	92.0	200.0	18.0	20
EC (μS/cm)	498.0	892.0	687.0	-	140.0	20
TDS (mg/L)	309.0	558.0	428.0	1500.0	90.0	21
pH	6.4	7.1	6.6	8.5	0.2	3
TH (mg/L)	257.0	415.0	326.0	500.0	41.0	13
CAI	–0.1	0.4	0.1	-	0.1	1
SI-calcite	–0.7	–0.2	–0.4		0.1	30
SI-dolomite	–1.8	–0.8	–1.0		0.3	25
SI-gypsum	–2.3	–1.3	–1.9		0.3	13
SI-halite	–7.7	–6.5	–7.0		0.4	5
$\delta^{18}O$-H_2O (‰)	–6.3	–4.8	–5.5		0.5	9
$\delta^{2}H$-H_2O (‰)	–28.7	–20.7	–24.7		2.0	10
$\delta^{15}N$-NO_3^- (‰)	6.0	11.3	8.7		2.0	20
$\delta^{18}O$-NO_3^- (‰)	1.6	5.9	3.4		1.0	41

Note: WHO, World Health Organization. -, not available. EC, electrical conductivity; TH, total hardness; TDS, total dissolved solids; CAI, chloro-alkaline index; SI-calcite, SI-dolomite, SI-gypsum, and SI-halite represent the saturation indices of calcite, dolomite, gypsum, and halite, respectively.

2), were collected from this aquifer (samples 1, 2, and 6). The groundwater pH value was slightly acidic, where it ranged between 6.6 and 6.7 with an average of 6.6. EC value was in the range of 617.0–821.0 μS/cm with an average of 743.0 μS/cm (Fig. 4). Based on the classification of Davis and De Wiest (1967), we classified the groundwater as freshwater, where TDS content was in the range of 385.0–519.0 mg/L with an average of 466.0 mg/L. Based on Sawyer and McCarty classification (1968), we categorized the groundwater as very hard water, where TH value was in the range of 333.0–366.0 mg/L with an average of 344.0 mg/L as $CaCO_3$. Based on TDS and TH values, we described the groundwater of A1/2 aquifer as fresh-very hard water. Mg^{2+} and Ca^{2+} concentrations ranged from 22.8 to 37.7 mg/L with an average of 28.3 mg/L, and from 71.8 to 109.0 mg/L with an average of 91.3 mg/L, respectively. Na^+ and K^+ concentrations ranged from 26.5 to 78.7 mg/L with an average of 53.4 mg/L, and from 1.3 to 6.0 mg/L with an average of 3.6 mg/L, respectively. HCO_3^- and SO_4^{2-} concentrations ranged from 160.0 to 176.0 mg/L with an average of 168.0 mg/L, and from 25.5 to 56.2 mg/L with an average of 44.2 mg/L, respectively. Cl^- concentration was in the range of 66.0–156.0 mg/L with an average of 107.0 mg/L. All of the above-mentioned parameters for all samples fell within the permissible limit set by the WHO (2011). NO_3^- concentration ranged from 18.5 to 65.0 mg/L with an average of 39.7 mg/L. All samples have NO_3^- concentration above the natural background of natural source of 5.0–10.0 mg/L (Panno et al., 2006). One sample (Sample 1) has NO_3^- concentration exceeding the permissible maximum limit of drinking water quality of 50.0 mg/L set by the WHO (2011). Potential sources of groundwater contamination in the study area are sewerage, solid waste, and slaughterhouses (Margane et al., 2010).

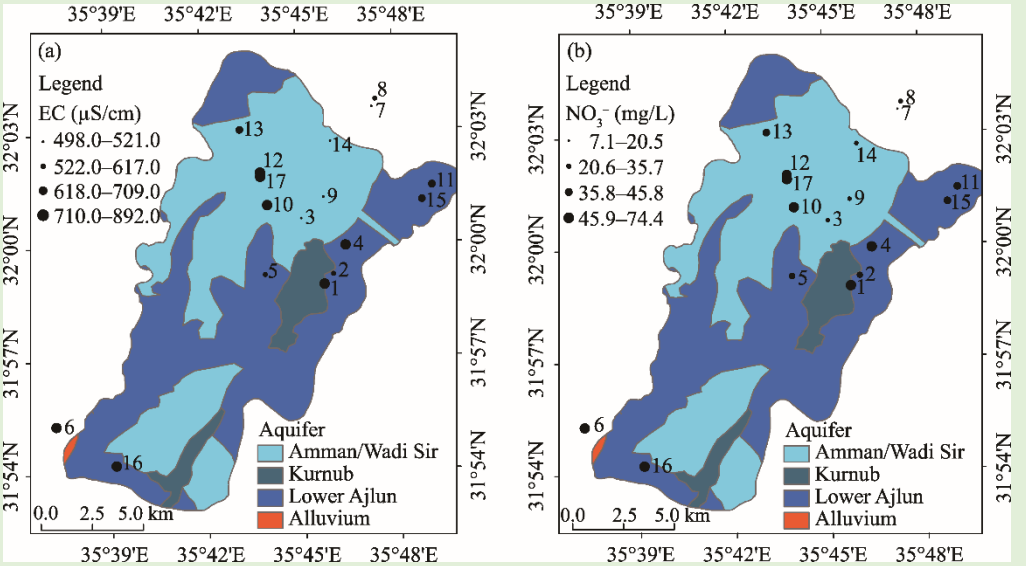

Fig. 4 Spatial distribution of electrical conductivity (EC) (a) and nitrate (NO_3^-) concentration (b)

3.1.2 Hummar aquifer (A4)

Seven water samples, with four from production wells (samples 8, 13, 14, and 16) and three from springs (samples 4, 11, and 15), were collected from this aquifer (samples 4, 8, 11, 13, 14, 15, and 16). In terms of pH value, the groundwater of this aquifer was similar to the groundwater of A1/2 aquifer; it was slightly acidic, where pH value ranged from 6.4 to 6.8 with an average of 6.6. EC value was in the range of 521.0–868.0 μS/cm with an average of 691.0 μS/cm. The groundwater is freshwater, where the TDS content was in the range of 323.0–541.0 mg/L with an average of 430.0 mg/L. It is hard-very hard water with TH value ranging from 279.0–414.0 mg/L with an average of 341.0 mg/L. Mg^{2+} and Ca^{2+} concentrations ranged from 12.0–40.0 mg/L with an average of 22.6 mg/L, and from 77.0 to 137.0 mg/L with an average of 99.4 mg/L, respectively. Na^+ and K^+ concentrations ranged from 24.0 to 78.0 mg/L with an average of 44.0 mg/L, and from 1.0 to 6.0 mg/L with an average of 2.0 mg/L, respectively. HCO_3^- and SO_4^{2-} concentrations ranged from 104.0–176.0 mg/L with an average of 154.0 mg/L, and from 24.0 to 118.0 mg/L with an average of 54.2 mg/L, respectively. Cl^- concentration was in the range of 42.0–148.0 mg/L with an average of 85.5 mg/L. All of the above-mentioned parameters for all samples fell within the permissible limit set by the WHO (2011). NO_3^- concentration ranged from 21.0 to 44.0 mg/L with an average of 32.2 mg/L. All samples had NO_3^- concentration above the natural background of natural source of 5.0–10.0 mg/L (Panno et al., 2006), and below the maximum permissible limit of drinking water quality set by the WHO (2011).

3.1.3 Amman formation/Wadi Es Sir aquifer (B2/A7)

Seven water samples, with one from production well (sample 7) and six from springs (samples 3, 5, 9, 10, 12, and 17) were collected from this aquifer (samples 3, 5, 7, 9, 10, 12, and 17). In terms of pH value, the groundwater of this aquifer was similar to the groundwater of A1/2 and A4 aquifers; it was slightly acidic, where pH value ranged from 6.4 to 7.1 with an average of 6.6. EC value was in the range of 498.0–892.0 μS/cm with an average of 660.0 μS/cm. The groundwater is freshwater, where the TDS content was in the range of 309.0–558.0 mg/L with an average of 410 mg/L. It is hard-very hard water with TH value ranging from 257.0 to 360.0 mg/L with an average of 303.0 mg/L. Mg^{2+} and Ca^{2+} concentrations ranged from 15.0 to 32.0 mg/L with an average of 22.6 mg/L, and from 62.0 to 101.0 mg/L with an average of 84.0 mg/L, respectively. Na^+ and K^+ concentrations ranged from 22.0 to 81.0 mg/L with an average of 47.6 mg/L, and from 1.0 to 14.0 mg/L with an average of 5.8 mg/L, respectively. HCO_3^- and SO_4^{2-} concentrations ranged from 148.0 to 180.0 mg/L with an average of 157.7 mg/L, and from 22.0 to 93.0 mg/L with an average of 51.1 mg/L, respectively. Cl^- concentration was in the range of 33.0–134.0 mg/L with an average

of 80.7 mg/L. All of the above-mentioned parameters for all samples fell within the permissible limit set by the WHO (2011). NO_3^- concentration ranged from 7.0 to 74.0 mg/L with an average of 41.2 mg/L. One sample (sample 7) had NO_3^- concentration within the natural background concentration of natural source of 5.0–10.0 mg/L (Panno et al., 2006), and two samples (samples 12 and 17) exhibited concentration above the maximum permissible limit of drinking water quality set by the WHO (2011).

3.2 Hydrochemical facies and processes

The distribution of the major ions of the groundwater in the Wadi Shueib catchment area showed the following patterns: (1) for the whole aquifer system, $Ca^{2+}>Na^+>Mg^{2+}>K^+$ and HCO_3^->Cl^->SO_4^{2-}>NO_3^-; (2) for the A1/2 aquifer, $Ca^{2+}>Na^+>Mg^{2+}>K^+$ and $Cl^->HCO_3^->SO_4^{2-}>NO_3^-$; and (3) for the A4 and B2/A7 aquifers, $Ca^{2+}>Na^+>Mg^{2+}>K^+$ and $HCO_3^->Cl^->SO_4^{2-}>NO_3^-$. Among the major ions, K^+ had the highest variation (coefficient of variation (CV)=109%), followed by SO_4^{2-} (CV=57%), NO_3^- (CV=47%), Na^+ (CV=46%), and Cl^- (CV=43%). This may indicate multiple sources and hydrogeochemical and mixing processes controlling the spatial distribution of the groundwater quality (Masoud, 2014). Correlation coefficients are commonly used to find out relationships between physiochemical parameters of the groundwater, and to demonstrate how well a parameter predicts the others (Islam et al., 2018; Bodrud-Doza et al., 2019). The bivariate statistics (Pearson correlation coefficient) of the physiochemical parameters of the groundwater in the study area are presented in Table 3. A very positive significant correlation was found among EC value and each concentration of Na^+, Cl^-, SO_4^{2-}, and K^+, indicating that the TDS value of the groundwater was mainly controlled by these ions. A moderate correlation was found between EC value and each concentration of NO_3^- and Ca^{2+}, which indicated that the more mineralization of the groundwater, the higher the chance for nitrate contamination and accumulation. The significant positive correlations of K^+ concentration with each concentration of Na^+, NO_3^-, and SO_4^{2-} indicated a common source of these ions in the groundwater, most likely domestic wastewater. A moderate negative correlation (–0.50) was found between Ca^{2+} and Mg^{2+} concentrations, indicating different sources of these ions. Potential sources of Mg^{2+} in the groundwater are animal and domestic waste (Selvam et al., 2016), whereas the source of Ca^{2+} is calcite dissolution, which is the main mineral in the aquifers under consideration. The moderate correlation (0.50) between NO_3^- and Cl^- concentrations indicated a common source, most likely animal and human waste.

Piper diagram presentation of the major ions revealed that most of the samples are of mixed Ca-Mg-Cl type, and only three samples (sample 8 of A4 aquifer, and samples 7 and 9 of B2/A7 aquifer) are of Ca-HCO_3 type (Fig. 5). Samples 7 and 8 were taken from two wells with a depth of 283 and

Table 3 Bivariate statistics of the hydrochemical parameters of the groundwater samples

Parameter	NO_3^-	Cl^-	SO_4^{2-}	HCO_3^-	Na^+	K^+	Mg^{2+}	Ca^{2+}	EC	pH	TH	^{18}O-H_2O	^{2}H-H_2O	^{15}N-NO_3^-	^{18}O-NO_3^-
NO_3^-	1.0	0.5	0.4	0.0	0.6	0.7	0.0	0.3	0.6	–0.3	0.3	0.7	0.6	0.5	–0.1
Cl^-	0.5	1.0	0.7	0.3	1.0	0.6	0.5	0.3	0.9	–0.4	0.7	0.7	0.8	0.7	0.2
SO_4^{2-}	0.4	0.7	1.0	0.4	0.8	0.7	0.2	0.6	0.9	–0.6	0.8	0.8	0.8	0.7	0.2
HCO_3^-	0.0	0.3	0.4	1.0	0.3	0.2	0.3	0.3	0.4	–0.1	0.5	0.1	0.1	0.5	0.3
Na^+	0.6	1.0	0.8	0.3	1.0	0.8	0.5	0.3	1.0	–0.4	0.7	0.8	0.9	0.7	0.1
K^+	0.7	0.6	0.7	0.2	0.8	1.0	0.2	0.3	0.7	–0.4	0.5	0.7	0.7	0.5	–0.2
Mg^{2+}	0.0	0.5	0.2	0.3	0.5	0.2	1.0	–0.5	0.4	–0.2	0.2	0.1	0.1	0.1	0.2
Ca^{2+}	0.3	0.3	0.6	0.3	0.3	0.3	–0.5	1.0	0.5	–0.4	0.8	0.4	0.4	0.7	0.2
EC	0.6	0.9	0.9	0.4	1.0	0.7	0.4	0.5	1.0	–0.5	0.9	0.8	0.8	0.8	0.2
pH	–0.3	–0.4	–0.6	–0.1	–0.4	–0.4	–0.2	–0.4	–0.5	1.0	–0.5	–0.4	–0.4	–0.4	–0.1
TH	0.3	0.7	0.8	0.5	0.7	0.5	0.2	0.8	0.9	–0.5	1.0	0.6	0.5	0.8	0.4
^{18}O-H_2O	0.7	0.7	0.8	0.1	0.8	0.7	0.1	0.4	0.8	–0.4	0.6	1.0	1.0	0.6	–0.1
^{2}H-H_2O	0.6	0.8	0.8	0.1	0.9	0.7	0.1	0.4	0.8	–0.4	0.5	1.0	1.0	0.6	0.0
^{15}N-NO_3^-	0.5	0.7	0.7	0.5	0.7	0.5	0.1	0.7	0.8	–0.4	0.8	0.6	0.6	1.0	0.6
^{18}O-NO_3^-	–0.1	0.2	0.2	0.3	0.1	–0.2	0.2	0.2	0.2	–0.1	0.4	–0.1	0.0	0.6	1.0

285 m, respectively. The first type (Ca-Mg-Cl type) can be related to the fourth group of Geyh et al. (1986), which corresponded to fresh water mixed with saline water or fresh water which has passed through evaporates. However, this water tended to shift towards the second type (Ca-HCO_3 type), which indicated mixing between two end members: one fresh (Ca-HCO_3) water and another one saline (Na-Cl) water (Panagopoulos et al., 2005). Ca-Mg-Cl water type can be interpreted as a mixture of high salinity water produced by surface contamination (e.g., domestic wastewater and septic effluents) with the existing water followed by ion exchange reactions (Selvam et al., 2016). The Ca-HCO_3 water type can be considered as the natural background water in the study area. Such type of water can evolve from the dissolution of carbonate rocks and it can be influenced by rainfall infiltration or dissolution of atmospheric carbon dioxide (Ayadi et al., 2018; Ligavha-Mbelengwa and Gomo, 2020). Most of the samples plotted in the Ca-dominant zone in the cation facies, followed by the no dominant zone (no one cation-anion pair exceeded 50%). Moreover, most of the samples fell in the no dominant zone in the anion zone (no one cation-anion pair exceeded 50%), with some samples fell in the HCO_3 and Cl zones.

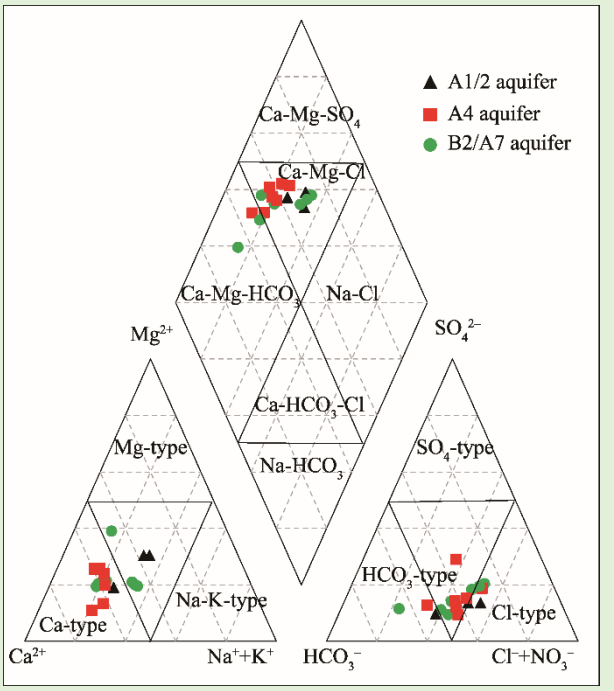

Fig. 5 Piper diagram of the groundwater samples in the study area. A1/2, Na'ur aquifer; A4, Hummar aquifer; B2/A7, Amman/Wadi Wadi Es Sir aquifer.

The relationships between the dissolved ions have been extensively used to track salinity sources and evolution of the groundwater (Thilakerathne et al., 2015; Senarathne et al., 2019; Tiwari et al., 2019). The ratio of the HCO_3^- to ΣAnions for the groundwater samples in the study area ranged from 0.27 to 0.65 with an average of 0.41. These values indicated rock weathering, especially carbonate rocks (Halim et al., 2010; Bodrud-Doza et al., 2019).

The ratio between Na^+ and Cl^- concentrations has been used to identify sources of salinity, silicate weathering, seawater intrusion, halite dissolution, and ion exchange processes (Garcia et al., 2001; Rubasinghe et al., 2015). The Na^+/Cl^- ratio in the groundwater samples in the study area ranged from 0.60 to 1.00 with an average of 0.84. About 47% of the samples had Na^+/Cl^- ratio above the seawater ratio of 0.86 (Mercado, 1985), and close to 1.00, indicating contamination by domestic wastewater or water-rock-interaction (Zhu et al., 2010; Abdalla, 2016). Plot of Na^+/Cl^- ratio vs Cl^- can be used to identify sources of salinity in the groundwater, where Na^+/Cl^- ratio should be equal to 1.00 if halite is the source of these ions, and other mechanisms such as salt water intrusion, and ion exchange process and rock-water interaction should be the sources, if the Na^+/Cl^-

ratio departs from 1.00 (Basins and Geo, 2004; Abu-alnaeem et al., 2018; Tiwari et al., 2019). The Na^+/Cl^- ratio of wastewater taken from Al-Salt wastewater treatment was about 1.03 (Al-Kharabsheh and Al-Kharabsheh, 2014). Except sample 7 (B2/A7 aquifer), which is of Ca-HCO_3 type, all other samples from the study area had a Na^+/Cl^- ratio below 1.00 (Fig. 6a). This may indicate mixing with more saline water (Ayadi et al., 2018), and reverse ion exchange process (Abu-alnaeem et al., 2018). Moreover, the HCO_3^-/Cl^- ratio can be used to indicate freshwater recharge (Ayadi et al., 2018). The HCO_3^-/Cl^- ratio of the groundwater samples used in the present study ranged from 0.63 to 3.19, with about 65% of the samples having a HCO_3^-/Cl^- ratio above 1.00, indicating freshwater recharge (Fig. 6b). Mixing processes, may be with wastewater, led to a decrease in the HCO_3^-/Cl^- ratio for those samples having HCO_3^-/Cl^- ratio less than 1.00. The relationship between Cl^- and Ca^{2+}/Na^+ ratio (Fig. 6c) showed that the Ca^{2+}/Na^+ ratio was greater than 1.00, indicating aquifer carbonate dissolution or depletion of Na^+ (Ayadi et al., 2018). The Ca^{2+}/HCO_3^- ratio can be used to evaluate carbonate dissolution. If the calcite dissolution is dominant, the Ca^{2+}/HCO_3^- ratio should be close to 1.00, and if dolomite dissolution is dominant, the Ca^{2+}/HCO_3^- ratio should be close to 0.50 (Abu-alnaeem et al., 2018). Plot of Ca^{2+}/HCO_3^- ratio vs Cl^- indicated that all samples from the Wadi Shueib fell above Ca^{2+}/HCO_3^- ratio of 1.00 (Fig. 6d), indicating calcite dissolution. The excess in Ca^{2+} can be attributed to reverse ion exchange (Tiwari et al., 2019).

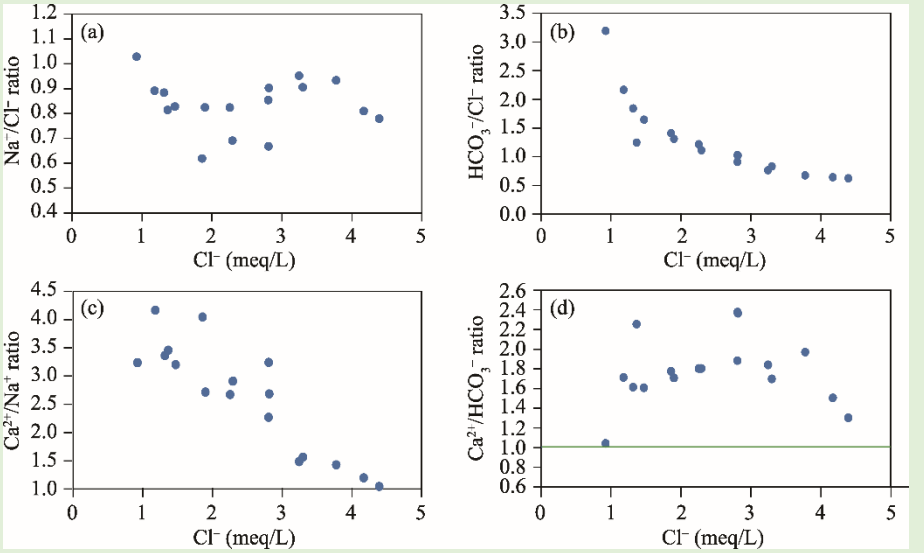

Fig. 6 Plots of Cl^- vs. Na^+/Cl^- ratio (a), Cl^- vs. HCO_3^-/Cl^- ratio (b), Cl^- vs Ca^{2+}/Na^+ ratio (c), and Cl^- vs. Ca^{2+}/HCO_3^- ratio (d). The green solid line indicates the molar ratio of calcite dissolution.

The SI-calcite of the groundwater samples ranged from –0.7 to –0.2 with an average of –0.4, and the SI-dolomite ranged from –1.8 to –0.8 with an average of –1.0 (Table 2). Moreover, the SI of gypsum and halite showed negative values, where it ranged from –2.3 to –1.3 with an average value of –1.9, and from –7.7 to –6.5 with an average of –7.0, respectively. These values indicate that the groundwater is unsaturated with respect to carbonate minerals, as well as evaporate minerals (Fig. 7), and dissolution of these minerals from the aquifer will lead to an increase in the TDS content of the groundwater in the study area.

The CAI values of the groundwater in the Wadi Shueib ranged from –0.1 to 0.4 with an average of 0.1 (Table 2; Fig. 8a). Most of the samples had positive CAI values, indicating hardening of the groundwater (release of the Ca^{2+} and Mg^{2+} ions into the water and sequestering of Na^+ and K^+ onto the aquifer material). This reaction was termed as reverse ion exchange process (Abu-alnaeem et al., 2018; Tiwari et al., 2019). Three samples (samples 7, 12, and 17 of B2/A7 aquifer) had a negative CAI, indicating softening process of the groundwater, and this reaction was termed as base ion exchange process (Tiwari et al., 2019). However, the positive values of CAI clustered between

0.0 and 0.2, indicating a low level of this process. Moreover, the cation exchange was confirmed by plotting $(Na^{+}+K^{+})$–Cl^{-} vs. $(Ca^{2+}+Mg^{2+})$–$(SO_4^{2-}+HCO_3^{-})$, as shown in Figure 8b. The NO_3^{-}/Cl^{-} ratio can be used to discriminate the nitrate pollution sources (Anornu et al., 2017). If the groundwater is not affected by human activities, the NO_3^{-}/Cl^{-} ratio is in the range of 0.05–0.22. The NO_3^{-}/Cl^{-} ratio for the A1/2 aquifer ranged from about 0.10–0.37; for the A4 aquifer, it was in the range of 0.12–0.36; and for B2/A7, it was in the range of 0.12–0.37. These values indicated anthropogenic source of NO_3^{-} in the three aquifers. The values of NO_3^{-}/Cl^{-} tended to decrease with increasing Cl^{-} concentration, approaching the NO_3^{-}/Cl^{-} ratio for wastewater which was about 0.42.

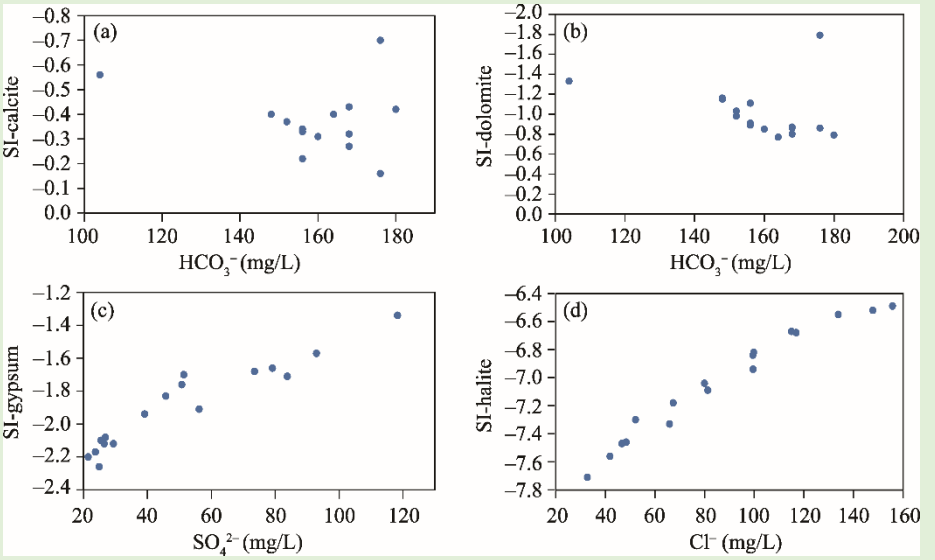

Fig. 7 Plots of SI-calcite vs. HCO_3^{-} (a), SI-dolomite vs. HCO_3^{-} (b), SI-gypsum vs. SO_4^{2-} (c), and SI-halite vs. Cl^{-} (d). SI-calcite, SI-dolomite, SI-gypsum, and SI-halite represent the saturation indices of calcite, dolomite, gypsum, and halite, respectively.

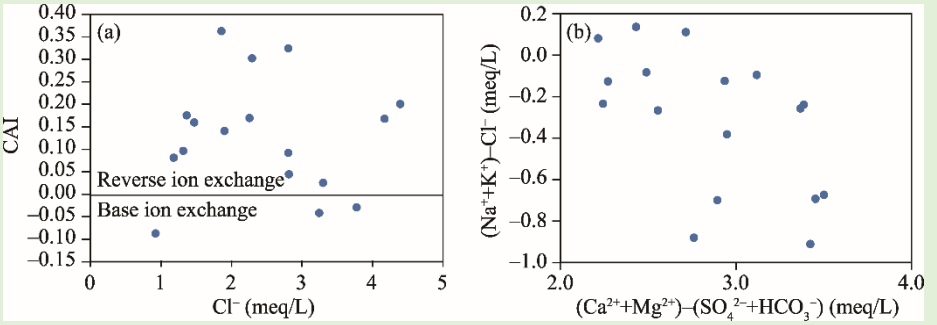

Fig. 8 Plots of CAI vs. Cl^{-} (a), and $(Na^{+}+K^{+})$–Cl^{-} vs. $(Ca^{2+}+Mg^{2+})$–$(SO_4^{2-}+HCO_3^{-})$ (b). The black solid line separates the two types of ion exchange (reverse ion exchange and base ion exchange).

3.3 $\delta^{2}H$ and $\delta^{18}O$ values of the groundwater

The stable isotope composition of water has been employed to investigate hydrological processes, such as infiltration, evaporation, and rock-water interaction (Clark and Fritz, 2013). The $\delta^{18}O$ and $\delta^{2}H$ values of the groundwater in the study area showed very slight variations (CV=8.5% for $\delta^{18}O$; CV=9.5% for $\delta^{2}H$), where the values ranged from –6.3‰ to –4.8‰ with an average of –5.5‰ for $\delta^{18}O$, and from –28.7‰ to –20.7‰ with an average of –24.7‰ for $\delta^{2}H$. The stable isotopic composition of the groundwater from the three aquifers (A1/2, A4, and B2/A7) was plotted using a ^{2}H-^{18}O diagram (Fig. 9). The stable isotopic composition of precipitation in Jordan, i.e., the Local Meteoric Water Line (LMWL; Bajjali, 2012), the Global Meteoric Water Line (GMWL), and the

Eastern Mediterranean Meteoric Water Line (MMWL) were also plotted. The $\delta^{18}O$ values of the precipitation in Jordan ranged from –7.3‰ to –3.5‰, and the $\delta^{2}H$ values ranged from –33.2‰ to –19.9‰. It can be seen that the $\delta^{18}O$ and $\delta^{2}H$ values of the groundwater samples fell close to local precipitation and the MMWL, indicating that the groundwater in the study area has been recharged from Mediterranean meteoric water. The samples were clustering along a well-defined local evaporation line (LEL), which fits the following equation:

$$\delta^{2}H = 4.89\delta^{18}O + 2.17 . \quad (6)$$

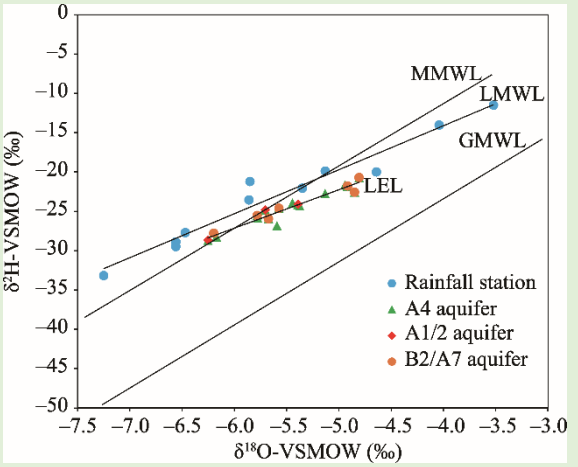

Fig. 9 Plot of $\delta^{18}O$-VSMOW vs. $\delta^{2}H$-VSMOW values of the groundwater samples. VSMOW, Vienna Standard Mean Ocean Water; MMWL, the Eastern Mediterranean Meteoric Water Line; LMWL, the Local Meteoric Water Line; LEL, the local evaporation line; GMWL, the Global Meteoric Water Line.

However, the samples were clustering in three groups. The first group had $\delta^{18}O$ and $\delta^{2}H$ values ranging from –5.1‰ to –4.8‰, and from –22.8‰ to –20.7‰, respectively. This group involved five samples, with two samples from A4 aquifer (samples 4 and 16) and three samples from B2/A7 aquifer (samples 10, 12, and 17), and it was isotopically enriched due to evaporation effect. The second group had $\delta^{18}O$ and $\delta^{2}H$ values ranging from –5.78‰ to –5.38‰, and from –26.84‰ to –23.97‰, respectively; it involved nine samples, with two samples from the A1/2 aquifer (samples 1 and 6), four samples from the A4 aquifer (samples 11, 13, 14, and 15), and three samples from the B2/A7 aquifer (samples 3, 5, and 9). The third group was relatively depleted in $\delta^{18}O$ and $\delta^{2}H$ values compared with the first and second groups. It had $\delta^{18}O$ and $\delta^{2}H$ values ranging from –6.3‰ to –6.2‰, and –28.7‰ to –27.8‰, respectively, and involved one sample from the A1/2 aquifer (sample 2), one sample from the A4 aquifer (sample 8), and one sample from the B2/A7 aquifer (sample 7). Samples 7 and 8 were taken from two wells with depth of 285 and 283 m, respectively, implying a well depth effect on the isotope composition of the groundwater. The air masses that produce rains in the Middle East come from different areas, such as the Siberian Plateau, the Northern Pole via Eastern Europe, Atlantic Ocean, the northern Africa and the Red Sea (Kattan, 2019). Bajjali (2012) showed that the cold and dry continental air masses stemming from the European continent come in contact with the warm Mediterranean Sea water, resulting in rapid evaporation and large-scale convergence. The deuterium excess (*d*-parameter) of the groundwater ($d=2\times\delta^{2}H-8\times\delta^{18}O$) ranged from 16.2‰ to 21.8‰ with an average of 19.3‰, which is slightly lower than that of the local precipitation (ranging from 16.6‰ to 25.6‰ with an average of 21.7‰). Variation in the *d*-parameter may indicate mixing of water from different sources having different isotopic signatures (El-Sayed et al., 2018). A single-factor analysis of variance test (ANOVA) was performed to find out if there is a significant difference between the $\delta^{18}O$ and $\delta^{2}H$ values for the samples collected from the three aquifer units. The test showed no significant difference in $\delta^{18}O$ values for A/2 and A4 aquifers, because the *F*-calculated value (1.14) was smaller than the *F*-critical value (5.32), and the *P*-value obtained (0.32) was greater than 0.05. The test revealed also

no significant difference in $\delta^{18}O$ values for A/2 and B2/A7 aquifers, as the *F*-calculated value (1.04) was smaller than the *F*-critical value (5.32), and the *P*-value calculated (0.34) was greater than 0.05. The test showed no significant difference in $\delta^{18}O$ for A4 and B2/A7 aquifers, because the *F*-calculated value (0.12) is smaller than the *F*-critical value (4.75), and the *P*-value obtained (0.73) is greater than 0.05. The test clearly indicated that the groundwater of the three aquifers have the same recharging sources, that is Mediterranean rainfall.

The relationship of $\delta^{18}O$ values with Cl^- concentration in the three aquifers (A1/2, A4, and B2/A7) is depicted in Figure 10a, where a very significant correlation was found for the A4 aquifer (r=0.92) and for the B2/A7 aquifer (r=0.98), indicating a strong evaporation effect. A moderate correlation (r=0.51) was found for the A1/2 aquifer, indicating a moderate evaporation effect. The relationship between $\delta^{18}O$ values and the *d*-parameter of the groundwater in the Wadi Shueib is presented in Figure 10b. The three aquifers exhibited very significant correlations (r=0.98 for the A1/2 aquifer; r=0.84 for the A4 aquifer; and r=0.96 for the B2/A7 aquifer) between $\delta^{18}O$ values and the *d*-parameter, indicating a strong evaporation effect on the isotopic composition of the groundwater.

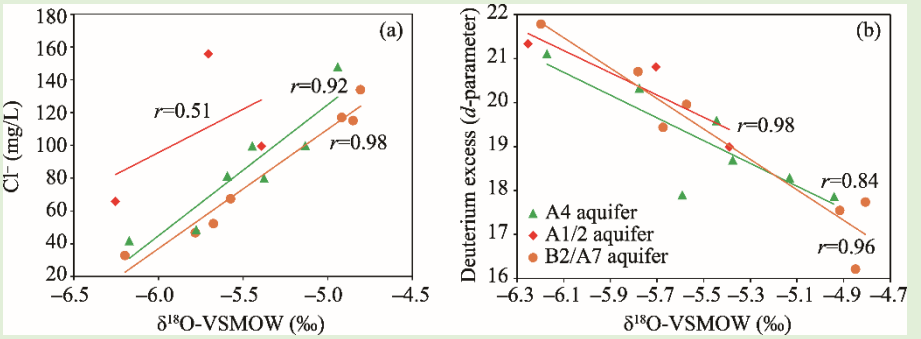

Fig. 10 Plots of $\delta^{18}O$-VSMOW vs. Cl^- (a) and $\delta^{18}O$-VSMOW vs. deuterium excess (*d*-parameter) (b)

3.4 ^{15}N-NO_3^- and ^{18}O-NO_3^- values of the groundwater

The $\delta^{15}N$-NO_3^- values of the groundwater in the study area ranged from 6.0‰ to 11.3‰ with an average of 8.7‰, and the $\delta^{18}O$-NO_3^- values ranged from 1.6‰ to 5.9‰ with an average of 3.4‰ (Table 2). The $\delta^{15}N$-NO_3^- and $\delta^{18}O$-NO_3^- values of the A1/2 aquifer ranged from 9.0‰ to 11.3‰ with an average of 9.9‰, and from 4.0‰ to 5.9‰ with an average of 4.9‰, respectively. The A4 aquifer had $\delta^{15}N$-NO_3^- and $\delta^{18}O$-NO_3^- values in the range of 6.0‰–11.1‰ with an average of 8.6‰, and in the range of 1.8‰–5.8‰ with an average of 3.4‰, respectively. The B2/A7 aquifer had $\delta^{15}N$-NO_3^- and $\delta^{18}O$-NO_3^- values in the range of 6.1‰–10.4‰ with an average of 8.3‰, and in the range of 1.6‰–4.8‰ with an average of 2.8‰, respectively. The relationship plot of $\delta^{15}N$ and $\delta^{18}O$ was used to identify the sources of the nitrate in the study area (Fig. 11) (Kendall et al., 2007). About 59% of the samples (samples 1, 2, 4, 5, 6, 10, 11, 12, 16, and 17) fell in the source "manure/septic waste" window. These samples represented the three aquifers in the study area: samples 1, 2, and 6 of the A1/2 aquifer, samples 4, 11, and 16 of the A4 aquifer, and samples 5, 10, 12, and 17 of the B2/A7 aquifer. These samples had $\delta^{15}N$-NO_3^- values in the range of 8.6‰ to 11.3‰, and $\delta^{18}O$-NO_3^- values in the range of 1.6‰ to 5.9‰, which are in compliance with the stable isotopic composition of nitrate derived the nitrification of wastewater/manure (Widory et al., 2004; Kendall et al., 2007; Xue et al., 2009; Adebowale et al., 2019; Danni et. al., 2019; Zhang and Wang, 2020). The $\delta^{15}N$-NO_3^- and $\delta^{18}O$-NO_3^- values of the wastewater in the study area were 9.3‰ and 7.4‰, respectively (Grimmeisen et al., 2017). The NO_3^- concentration of the above samples ranged from 19.0 to 74.0 mg/L, which is above the natural background concentration of NO_3^- (5.0–10.0 mg/L) (Panno et al., 2006). Thus, the source of this group of samples can be considered manure/septic waste. In addition, the stable isotopic composition of seven samples (samples 3, 7, 8, 9, 13, 14, and 15) fell in the crossing window of the sources manure/septic waste and soil NH_4. The $\delta^{15}N$-NO_3^- values of these samples ranged from 6.0‰ to 7.8‰, and the $\delta^{18}O$-NO_3^- values

ranged from 1.8‰ to 3.1‰. Except sample 7 which had NO_3^- concentration (7.0 mg/L) within the natural background concentration (5.0–10.0 mg/L), the NO_3^- concentration of this group of samples ranged from 26.0 to 39.0 mg/L, which is higher than the natural background concentration. Sample 7 was collected from a well tapping the B2/A7 aquifer (well depth of 283 m), and it had $\delta^{15}N\text{-}NO_3^-$ and $\delta^{18}O\text{-}NO_3^-$ values of 6.1‰ and 2.6‰, respectively. Samples 3 and 9 were collected from the B2/A7 aquifer, and samples 8, 13, 14, and 15 were collected from the A4 aquifer. Accordingly, nitrate isotope composition of sample 7 indicated soil NH_4 origin of nitrate, whereas samples 3, 8, 9, 13, 14, and 15 had wastewater/manure source of nitrate. This is supported by the results of the analysis of total coliform and *Escherichia coli* reported by several researches carried out in the study area (Al-Kharabsheh and Al-Kharabsheh, 2014). Average values of total coliform were found to be in the range of 10.1–11,741.7 MPN/100 mL in ten springs in the study area (Al-Kharabsheh and Al-Kharabsheh, 2014). These springs had the following samples in this study: samples 1 and 2 of the A1/2 aquifer; samples 3, 5, 9, 10, 12, and 17 of the B2/A7 aquifer; and samples 4 and 11 of the A4 aquifer. *Escherichia coli* was also detected in three springs with values as follows: 5.0 MPN/100 mL for sample 5, 13.0 MPN/100 mL for sample 3, and 110.0 MPN/100 mL for sample 10 (Zemann et al., 2015). All these springs emerge from the B2/A7 aquifer.

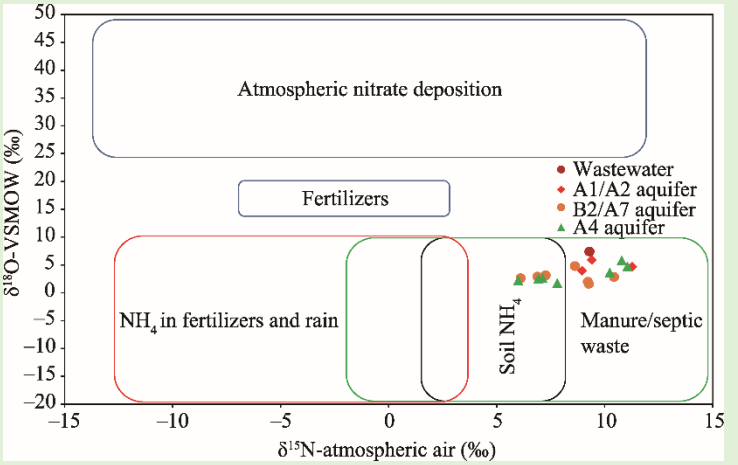

Fig. 11 Plot of $\delta^{15}N$-atmospheric air vs. $\delta^{18}O$-VSMOW of the groundwater samples in the study area. The stable isotopic composition of nitrate in wastewater in the study area is also presented.

Choride has been used as a conservative tracer of groundwater contamination (Koh et al., 2010; Baily et al., 2011; Jiang et al., 2016; Anornu et al., 2017). Plotting Cl^- concentration vs. $\delta^{15}N$-atmospheric air revealed a significant correlation (r=0.73), indicating that manure/septic waste is a major source of nitrate of groundwater in the study area (Fig. 12a).

A single-factor analysis of variance test (ANOVA) was performed to find out if there is a significant difference between the $\delta^{15}N\text{-}NO_3^-$ and $\delta^{18}O\text{-}NO_3^-$ values for the three aquifers. The test showed no significant difference between the $\delta^{15}N\text{-}NO_3^-$ values for the A1/2 and A4 aquifers, as the F-calculated value (2.55) was smaller than the F-critical value (5.32), and the P-value calculated (0.15) was greater than 0.05. No significant difference was found between the $\delta^{15}N\text{-}NO_3^-$ values for the A1/2 and B2/A7 aquifers, as the F-calculated value (1.01) was smaller than the F-critical value (5.32), and the P-value calculated (0.34) was greater than 0.05. No significant difference was found between the $\delta^{15}N\text{-}NO_3^-$ values for the A4 and B2/A7 aquifers, as the F-calculated value (0.10) was smaller than the F-critical value (4.75), and the P-value calculated (0.76) was greater than 0.05. The ANOVA test revealed a significant difference between the $\delta^{18}O\text{-}NO_3^-$ values for the A1/2 and A4 aquifers, since the F-calculated value (8.36) was greater than the F-critical value (5.32), and the P-value calculated (0.02) was smaller than 0.05. The test revealed no significant difference between the $\delta^{18}O\text{-}NO_3^-$ values for the A1/2 and B2/A7 aquifers, as the F-calculated (2.53) was smaller than the F-critical (5.32), and the P-value calculated (0.10) was greater than 0.05. The test also showed no significant difference between the $\delta^{18}O\text{-}NO_3^-$ values for the A4

aquifer and the $\delta^{18}O\text{-}NO_3^-$ values for the B2/A7 aquifer, because the *F*-calculated value (0.57) was smaller than the *F*-critical value (4.75), and the *P*-value calculated (0.47) was greater than 0.05. The results of the ANOVA test indicated that the three aquifer units (A1/2, A4, and B2/A7) have a common source of nitrate, primarily domestic wastewater.

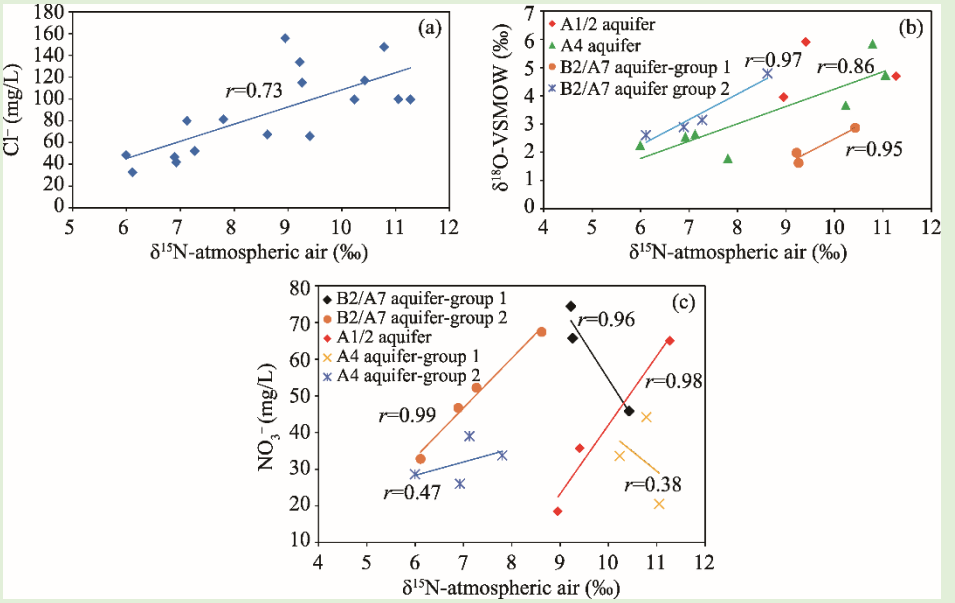

Fig. 12 Plots of $\delta^{15}N$-atmospheric air vs. Cl^- (a), $\delta^{15}N$-atmospheric air vs. $\delta^{18}O$-VSMOW (b), and $\delta^{15}N$-atmospheric air vs. NO_3^- (c). The regression line and correlation coefficient are also presented.

Groundwater in the Wadi Shueib had $\delta^{18}O\text{-}NO_3^-$ values (average of 3.4‰) that were much lower than those for nitrate in fertilizers (17.0‰ to 25.0‰) and atmospheric nitrate (25.0‰ to more than 70.0‰). This indicated that nitrification was the main biological transformation process of nitrogen species, and nitrate was mainly derived from the nitrification of wastewater/manure. The $\delta^{18}O\text{-}NO_3^-$ values produced from nitrification should be in the range from –10.0‰ to 10.0‰, since water had $\delta^{18}O$ values in the range from –25.0‰ to 4.0‰, and atmospheric oxygen had a value of about 23.5‰ (Durka et al., 1994; Kendall et al., 2007). We calculated the theoretical $^{18}O\text{-}NO_3^-$ produced by microbial nitrification for the groundwater in the study area based on the measured $\delta^{18}O$ values of the groundwater, assuming $\delta^{18}O$ value of atmospheric oxygen of 23.5‰, according to the following equation (Kendall et al., 2007):

$$\delta^{18}O\text{-}NO_3^- = 2/3\left(\delta^{18}O\text{-}H_2O\right) + 1/3\left(\delta^{18}O\text{-}O_2\right). \quad (7)$$

The theoretical $\delta^{18}O\text{-}NO_3^-$ values in the groundwater resources in the study area ranged from 3.7‰ to 4.6‰ with an average of 4.2‰, which were higher than the measured $\delta^{18}O\text{-}NO_3^-$ values in the range of 1.6‰–5.9‰ with an average of 3.4‰. About 71% of the samples had theoretical $\delta^{18}O\text{-}NO_3^-$ values higher than the measured $\delta^{18}O\text{-}NO_3^-$ values. The high theoretical $\delta^{18}O\text{-}NO_3^-$ values can be attributed to the high $\delta^{18}O\text{-}H_2O$ values, which ranged from –6.3‰ to –4.8‰ with an average of –5.5‰, showing a strong evaporation effect. In general, the average measured $\delta^{18}O\text{-}NO_3^-$ value (3.4‰) was consistent with the average theoretical $\delta^{18}O\text{-}NO_3^-$ value (4.2‰) for nitrification.

The relationship between $\delta^{15}N\text{-}NO_3^-$ and $\delta^{18}O\text{-}NO_3^-$ values provided useful information about the denitrification process taking place within the aquifer. The relationship between $\delta^{15}N\text{-}NO_3^-$ and $\delta^{18}O\text{-}NO_3^-$ values for all samples (n=17) representing the three aquifers showed a moderate correlation (r=0.50). However, splitting the samples based on the aquifer source (Fig. 12b) revealed that there was a very significant correlation (r=0.86) between $\delta^{15}N\text{-}NO_3^-$ and $\delta^{18}O\text{-}NO_3^-$ for samples collected from the A4 aquifer (n=7). Two groups of samples can be observed: the first group included samples 4, 11, and 16. This group of samples had high values of $\delta^{15}N\text{-}NO_3^-$ (from

10.0‰ to 11.1‰) and $\delta^{18}O\text{-}NO_3^-$ (from 3.7‰ to 5.8‰). These values corresponded to nitrate derived from nitrification of manure/septic waste. The same group showed a moderate negative correlation (r= –0.38) between NO_3^- concentration and $\delta^{15}N$ values (Fig. 12c), signifying to denitrification. Thus, the isotopic data of this group indicated both source and process signals. The second group included samples 8, 13, 14, and 15. This group had $\delta^{15}N\text{-}NO_3^-$ and $\delta^{18}O\text{-}NO_3^-$ values in the range of 6.0‰–7.8‰ and in the range of 1.8‰–2.6‰, respectively. A moderate positive correlation existed (r=0.47) between NO_3^- concentration and $\delta^{15}N$ values (Fig. 12c). Additionally, two groups of samples (n=7) which were collected from the B2/A7 aquifer can be delineated. The first group covered samples 10, 12, and 17; these samples showed a very significant correlation (r=0.95) between $\delta^{15}N\text{-}NO_3^-$ and $\delta^{18}O\text{-}NO_3^-$ values. This group of samples had $\delta^{15}N\text{-}NO_3^-$ and $\delta^{18}O\text{-}NO_3^-$ values in the range of 9.2‰–10.4‰ and in the range of 1.6‰–2.9‰, respectively, which corresponded to nitrate derived from nitrification of manure/septic waste. A very significant negative correlation (r= –0.96) existed between NO_3^- concentration and $\delta^{15}N$ values for this group, which signified to denitrification (Fig. 12c). The second group covered samples 3, 5, 7, and 9. This group also showed a very significant correlation (r=0.97) between $\delta^{15}N\text{-}NO_3^-$ and $\delta^{18}O\text{-}NO_3^-$ values. A very significant positive correlation (r=0.99) existed between NO_3 concentration and $\delta^{15}N$ values for this group. The A1/2 aquifer showed no clear relationship between $\delta^{15}N\text{-}NO_3^-$ and $\delta^{18}O\text{-}NO_3^-$ values. A very significant positive correlation (r=0.98) existed between NO_3^- concentration and $\delta^{15}N$ values for the groundwater collected from this aquifer.

4 Conclusions

We used the conventional hydrochemical methods in conjunction with isotopic methods to investigate the groundwater chemistry evolution as well as sources of pollution in the Wadi Shueib catchment area. Groundwater is fresh, belonging to hard to very hard water. Results revealed that dissolution of the aquifer minerals as well as reverse ion exchange are the main natural processes affecting groundwater chemistry in the study area. The stable isotopic composition of the groundwater ($\delta^2H\text{-}H_2O$ and $\delta^{18}O\text{-}H_2O$) showed that it is of meteoric origin, being recharged by Mediterranean rainfall, and undergoing strong evaporation. NO_3^- concentration signifies to contamination of the groundwater resources due to anthropogenic activities. Nitrate isotopes ($^{15}N\text{-}NO_3^-$ and $^{18}O\text{- }NO_3^-$) showed that nitrified wastewater/manure is the main source of contamination of the groundwater in the study area. No significant differences were found in the chemistry and isotopes values of the three aquifers, indicating that these aquifers are hydraulically interconnected and have common sources/processes influencing the water chemistry and pollution. Nitrification and denitrification are the main transformation processes of nitrogen species in the study area. Although the aquifer system is unconfined, denitrification might occur in anaerobic pockets within the aquifer. Hydrogeological interconnectivity between the three aquifer units was supported by the similar nitrate isotope contents of the three aquifers, as well as the results of the statistical tests. The use of nitrate isotopes in this study has given new insights into the sources of contamination of groundwater resources in the study area, an issue which cannot be tackled by only hydrochemical tools. Sustainable management of groundwater resources in the study area necessitates application of best management practices and proper land use planning. Connecting the study area to a sewerage system as preventive measure of water resources pollution is highly recommended. The results of the study are an important tool for decision makers to enact effective water protection policies.

Acknowledgements

This study was funded by the by the Deanship of Scientific Research, Jordan University of Science and Technology (20170338).

References

Abdalla F. 2016. Ionic ratios as tracers to assess seawater intrusion and to identify salinity sources in Jazan coastal aquifer, Saudi

Arabia. Arabian Journal of Geoscience, 9(1): 40, doi: 10.1007/s12517-015-2065-3.

Abu-alnaeem M F, Yusoff I, Ng T F, et al. 2018. Assessment of groundwater salinity and quality in Gaza coastal aquifer, Gaza Strip, Palestine: An integrated statistical, geostatistical and hydrogeochemical approaches study. Science of the Total Environment, 615: 972–989.

Adebowale T, Surapaneni A, Faulkner D, et al. 2019. Delineation of contaminant sources and denitrification using isotopes of nitrate near a wastewater treatment plant in peri-urban settings. Science of the Total Environment, 651: 2701–2711.

Al-Kharabsheh N M, Al-Kharabsheh A A. 2014. Influence of urbanization on water quality deterioration of northern wadi shu'eib catchment area springs, Jordan. The Jordan Journal of Earth and Environmental Sciences, 6(1): 29–35.

Anornu G, Gibrilla A, Adomako D. 2017. Tracking nitrate sources in groundwater and associated health risk for rural communities in the White Volta River basin of Ghana using isotopic approach ($\delta^{15}N$, $\delta^{18}O$-NO_3 and ^{3}H). Science of the Total Environment, 603–604: 687–698.

APHA (American Public Health Association). 1998. Standard Methods for the Examination of Water and Wastewater (20th ed.). Washington: American Public Health Association, 1–1214.

Aravinthasamy P, Karunanidhi D, Subramani T, et al. 2019. Fluoride contamination in groundwater of the Shanmuganadhi River basin (South India) and its association with other chemical constituents using geographical information system and multivariate statistics. Geochemistry, 80(4), 125555, doi: 10.1016/j.chemer.2019.125555.

Archana A, Thibodeau B, Geeraert N, et al. 2018. Nitrogen sources and cycling revealed by dual isotopes of nitrate in a complex urbanized environment. Water Research, 142: 459–470.

Argamasilla M, Barber J A, Andreo B. 2017. Factors controlling groundwater salinization and hydrogeochemical processes in coastal aquifers from southern Spain. Science of the Total Environment, 580: 50–68.

Awawdeh M, Al-Kharbsheh N, Obeidat M, et al. 2020. Groundwater vulnerability assessment using modified SINTACS model in Wadi Shueib, Jordan. Annals of GIS, doi: 10.1080/19475683.2020.1773535.

Ayadi R, Trabelsi R, Zouari K, et al. 2018. Hydrogeological and hydrochemical investigation of groundwater using environmental isotopes (^{18}O, ^{2}H, ^{3}H, ^{14}C) and chemical tracers: a case study of the intermediate aquifer, Sfax, southeastern Tunisia. Hydrogeology Journal, 26: 983–1007.

Baily A, Rock L, Watson C J, et al. 2011. Spatial and temporal variations in groundwater nitrate at an intensive dairy farm in south-east Ireland: Insights from stable isotope data. Agriculture, Ecosystems and Environment, 144(1): 308–318.

Bajjali W. 2012. Spatial variability of environmental isotope and chemical content of precipitation in Jordan and evidence of slight change in climate. Applied Water Science, 2: 271–283.

Basins C R, Geo J E. 2004. Identification and evolution of hydrogeochemical processes in the groundwater environment in an area of the Palar and Cheyyar River Basins, Southern India. Environmental Geology, 46: 47–60.

Biddau R, Cidu R, Da Pelo S, et al. 2019. Source and fate of nitrate in contaminated groundwater systems: Assessing spatial and temporal variations by hydrogeochemistry and multiple stable isotope tools. Science of the Total Environment, 647: 1121–1136.

Bodrud-Doza Md, Bhuiyan M A H, Didar-Ul Islam S M, et al. 2019. Hydrogeochemical investigation of groundwater in Dhaka City of Bangladesh using GIS and multivariate statistical techniques. Groundwater for Sustainable Development, 8: 226–244.

Chang C C, Kendall C, Silva S R, et al. 2003. Nitrate stable isotopes: tools for determining nitrate sources among different land uses in the Mississippi River Basin. Canadian Journal Fisheries and Aquatic Sciences, 59(12): 1874–1885.

Chen N, Peng B, Hong H, et al. 2013. Nutrient enrichment and N: P ratio decline in a coastal bay-river system in southeast China: The need for a dual nutrient (N and P) management strategy. Ocean and Coastal Management, 81: 7–13.

Choi J D, Jang S O, Choi B Y, et al. 2000. Monitoring study on groundwater quality of an alluvial plane in the north Han River basin. Journal of Korea of Water Quality, 16: 283–294.

Clague J C, Stenger R, Clough T J. 2015. Evaluation of the stable isotope signature of nitrate to detect denitrification in a shallow groundwater system in New Zealand. Agriculture, Ecosystems and Environment, 202: 188–197.

Clark I D, Fritz P. 2013. Environmental Isotopes in Hydrogeology. Boca Raton: CRC Press, 1–352.

Czekaj J, Jakobczyk-Karpierz S, Rubin H, et al. 2016. Identification of nitrate sources in groundwater and potential impact on drinking water reservoir (Goczalkowice reservoir, Poland). Physics and Chemistry of the Earth, 94: 35–46.

Danni S O, Bouchaou L, Elmouden A, et al. 2019. Assessment of water quality and nitrate source in the Massa catchment (Morocco) using $\delta^{15}N$ and $\delta^{18}O$ tracers. Applied Radiation and Isotopes, 154: 108859, doi: 10.1016/j.apradiso.2019.108859.

Davis S N, De Wiest J M. 1967. Hydrogeology. New York: John Wiley and Sons, 1–463.

Durka W, Schulze E D, Gebauer G, et al. 1994. Effects of forest decline on uptake and leaching of deposited nitrate determined

from ^{15}N and ^{18}O measurements. Nature, 372: 765–767.

El-Sayed S A, Morsy S M, Zakaria K M. 2018. Recharge sources and geochemical evolution of groundwater in the Quaternary aquifer at Atfih area, the northeastern Nile Valley, Egypt. Journal of African Earth Sciences, 142: 82–92.

Garcia G, Hidalgo V, Blesa A. 2001. Geochemistry of groundwater in the alluvial plain of Tucuman province, Argentina. Hydrogeology Journal, 9: 597–610.

Geyh M A, Rimawi O, Udluft P, et al. 1986. Environmental isotope study in the Hamad region. Natural water groups and their origin of the shallow aquifers complex in Azraq-depression, Jordan. The Hydrodynamic Pattern of the Central Part of Jordan. Geologisches Jahrbuch Reihe C, Band C38, 1–53.

Gold A J, DeRagon W R, Sullivan W M, et al. 1990. Nitrate-nitrogen losses to groundwater from rural and suburban land uses. Journal of Soil and Water Conservation, 45(2): 305–310.

Grimmeisen F, Lehmann M F, Liesch T, et al. 2017. Isotopic constraints on water source mixing, network leakage and contamination in an urban groundwater system. Science of the Total Environment, 583: 202–213.

GTZ (German Technical Cooperation). 1977. National Water Master Plan of Jordan: Groundwater Resources (Vol. 4). Groundwater Resources. Hanover: Federal Institute for Geosciences and Natural Resources.

Guo Z, Yan C, Wang Z, et al. 2020. Quantitative identification of nitrate sources in a coastal peri-urban watershed using hydrogeochemical indicators and dual isotopes together with the statistical approaches. Chemosphere, 243: 125364, doi: 10.1016/j.chemosphere.2019.125364.

Gutierrez M, Biagioni R N, Alarcon-Herrera M T, et al. 2018. An overview of nitrate sources and operating processes in arid and semiarid aquifer systems. Science of the Total Environment, 624: 1513–1522.

Halim M A, Majumder R K, Nessa S A, et al. 2010. Evaluation of processes controlling the geochemical constituents in deep groundwater in Bangladesh: Spatial variability on arsenic and boron enrichment. Journal Hazardous Materials, 180(1–3): 50–62.

Hoefs J. 2009. Stable Isotope Geochemistry. Berlin: Springer, 1–285.

Hu M M, Wang Y C, Du P C, et al. 2019. Tracing the sources of nitrate in the rivers and lakes of the southern areas of the Tibetan Plateau using dual nitrate isotopes. Science of the Total Environment, 658: 132–140.

Huan H, Hu L, Yang Y, et al. 2020. Groundwater nitrate pollution risk assessment of the groundwater source field based on the integrated numerical simulations in the unsaturated zone and saturated aquifer. Environmental International, 137: 105532, doi: 10.1016/j.envint.2020.105532.

Huang G, Sun J, Zhang Y, et al. 2013. Impact of anthropogenic and natural processes on the evolution of groundwater chemistry in a rapidly urbanized coastal area, south China. Science of the Total Environment, 463–464: 209–221.

Islam A R M T, Shen S, Haque M A, et al. 2018. Assessing groundwater quality and its sustainability in Joypurhat district of Bangladesh using GIS and multivariate statistical approaches. Environment, Development and Sustainability, 20: 1935–1959.

Jakobczyk-Karpierz S, Sitek S, Jakobsen R, et al. 2017. Geochemical and isotopic study to determine sources and processes affecting nitrate and sulphate in groundwater influenced by intensive human activity-carbonate aquifer Gliwice (southern Poland). Applied Geochemistry, 76: 168–181.

Jankowski K, Schnidler D E, Holtgrieve G W. 2012. Assessing nonpoint-source nitrogen loading and nitrogen fixation in lakes using delta N-15 and nutrient stoichiometry. Limnology and Oceanography, 57(3): 671–683.

Jawarneh R, Biradar C. 2017. Decadal national land cover database for Jordan at 30 m resolution. Arabian Journal of Geosciences, 10(22): 483, doi: 10.1007/s12517-017-3266-8.

Jeon C H. 2001. Effect of land use and urbanization on hydrochemistry and contamination of groundwater from Taejon area, Korea. Journal of Hydrology, 25(1–4): 194–210.

Jia H, Howard K, Qian H. 2020. Use of multiple isotopic and chemical tracers to identify sources of nitrate in shallow groundwaters along the northern slope of the Qinling Mountains, China. Applied Geochemistry, 113: 104512, doi: 10.1016/j.apgeochem.2019.104512.

Jiang W, Wang G, Sheng Y, et al. 2016. Enrichment and sources of nitrogen in groundwater in the Turpan-Hami area, northwestern China. Exposure and Health, 8: 389–400.

Johannsen A, Dähnke K, Emeis K. 2008. Isotopic composition of nitrate in five German rivers discharging into the North Sea. Organic Geochemistry, 39(12): 1678–1689.

Kaown D, Koh D C, Mayer B, et al. 2009. Identification of nitrate and sulfate sources in groundwater using dual stable isotope approaches for an agricultural area with different land use (Chuncheon, mid-eastern Korea). Agriculture, Ecosystems and Environment, 132(3–4): 223–231.

Kapelewska J, Kotowska U, Karpinska J, et al. 2019. Water pollution indicators and chemometric expertise for the assessment of the impact of municipal solid waste landfills on groundwater located in their area. Chemical Engineering Journal, 359: 790–800.

Karroum M, Elgettafi M, Elmandour A. 2017. Geochemical processes controlling groundwater quality under semi-arid environment: A case study in central Morocco. Science of the Total Environment, 609: 1140–1151.

Kattan Z. 2019. Factors controlling stable isotopes variability in precipitation in Syria: Statistical analysis approach. Journal of Earth System Science, 128: 151, doi: 10.1007/s12040-019-1142-5.

Kaushal S S, Groffman P M, Band L E. 2011. Tracking nonpoint source nitrogen pollution in human-impacted watersheds. Environmental Science and Technology, 45: 8225–8232.

Kendall C, Elliott E M, Wankel S D. 2007. Tracing anthropogenic inputs of nitrogen to ecosystems. In: Michener R H, Lajtha K. Stable Isotopes in Ecology and Environmental Science (2nd ed.). Oxford: Blackwell Publishing, 375–449.

Koh D C, Mayer B, Lee K S, et al. 2010. Land-use controls on sources and fate of nitrate in shallow groundwater of an agricultural area revealed by multiple environmental tracers. Journal of Contaminant Hydrology, 118(1–2): 62–78.

Kreitler C W. 1979. Nitrogen-isotope ratio studies of soils and groundwater nitrate from alluvial fan aquifers in Texas. Journal of Hydrology, 42(7): 147–170.

Kruk M K, Mayer B, Nightingale H, et al. 2020. Tracing nitrate sources with a combined isotope approach ($\delta^{15}N_{NO3}$, $\delta^{18}O_{NO3}$ and $\delta^{11}B$) in a large mixed-use watershed in southern Alberta, Canada. Science of the Total Environment, 703: 135043, doi: 10.1016/j.scitotenv.2019.135043.

Kuntz D. 2003. Soils in the Wadi Shueib catchment area and their protective potential for the Groundwater-Salt area. MSc Thesis. Karlsruhe: University of Karlsruhe.

Lee C M, Hamm S Y, Cheong J Y, et al. 2020. Contribution of nitrate-nitrogen concentration in groundwater to stream water in an agricultural head watershed. Environmental Research, 184: 109313, doi: 10.1016/j.envres.2020.109313.

Lee K S, Bong Y S, Lee D, et al. 2008. Tracing the sources of nitrate in the Han River watershed in Korea, using $\delta^{15}N\text{-}NO_3$ and $\delta^{18}O\text{-}NO_3$ values. Science of the Total Environment, 395(2–3): 117–124.

Lehmann M F, Simona M, Wyss S, et al. 2015. Powering up the "biogeochemical engine": the impact of exceptional ventilation of a deep meromictic lake on the lacustrine redox, nutrient, and methane balances. Frontier in Earth Science, 3: 45, doi: 10.3389/feart.2015.00045.

Levy Y, Shapira R H, Chefetz B, et al. 2017. Modeling nitrate from land surface to wells' perforations under agricultural land: success, failure, and future scenarios in a Mediterranean case study. Hydrology and Earth System Sciences, 21: 3811–3825.

Li C, Li S L, Yue F J, et al. 2020. Nitrate sources and formation of rainwater constrained by dual isotopes in Southeast Asia: Example from Singapore. Chemosphere, 241: 125024, doi: 10.1016/j.chemosphere.2019.125024.

Ligavha-Mbelengwa L, Gomo M. 2020. Investigation of factors influencing groundwater quality in a typical Karoo aquifer in Beaufort West town of South Africa. Environmental Earth Sciences, 79: 196, doi: 10.1007/s12665-020-08936-1.

MacDonald S M. 1965. East Bank Water Resources (Vol. 1–6). Amman: Central Water Authority.

Machiwal D, Cloutier V, Güler C, et al. 2018. A review of GIS-integrated statistical techniques for groundwater quality evaluation and protection. Environmental Earth Sciences, 77(19): 681, doi: 10.1007/s12665-018-7872-x.

Margane A, Subah A, Hamdan I, et al. 2009. Delineation of groundwater protection zones for the springs in wadi shuayb. In: Technical Report No. 14. Amman, Jordan.

Margane A, Subah A, Hamdan I, et al. 2010. Delineation of groundwater protection zones for the Wadi Shuayb springs. Technical Cooperation Project 'Groundwater Resources Management'. In: Technical Report No. 14. Amman, Jordan.

Martinelli G, Dadomo A, De Luca D A, et al. 2018. Nitrate sources, accumulation and reduction in groundwater from Northern Italy: Insights provided by a nitrate and boron isotopic database. Applied Geochemistry, 91: 23–35.

Masoud A A. 2014. Groundwater quality assessment of the shallow aquifers west of the Nile Delta (Egypt) using multivariate statistical and geostatistical techniques. Journal of African Earth Sciences, 95: 123–137.

Masri M. 1963. Report on the geology of the Amman, Zerqa area. Amman: Central Water Authority, 74.

Matiatos I. 2016. Nitrate source identification in groundwater of multiple land-use areas by combining isotopes and multivariate statistical analysis: A case study of Asopos basin (Central Greece). Science of the Total Environment, 541: 802–814.

Mattern S, Fasbender D, Vanclooster M. 2009. Discriminating sources of nitrate pollution in an unconfined sandy aquifer. Journal of Hydrology, 376(1–2): 275–284.

Mayer B, Boyer E W, Goodale C, et al. 2002. Sources of nitrate in rivers draining sixteen watersheds in the northeastern U.S.: Isotopic constraints. Biogeochemistry, 57–58: 171–197.

Mcilvin M, Altabet M. 2005. Chemical conversion of nitrate and nitrite to nitrous oxide for nitrogen and oxygen isotopic analysis in freshwater and seawater. Analytical Chemistry, 77(17): 5589–5595.

Megdal S B, Gerlak A K, Huang L Y, et al. 2017. Innovative approaches to collaborative groundwater governance in the United States: Case studies from three high-growth regions in the Sun Belt. Environmental Management, 59(5): 718–735.

Mercado A. 1985. Use of hydrogeochemical patterns in carbonate, sand and sandstone aquifers to identify intrusion and flushing saline water. Groundwater, 23(5): 635–645.

Mikbel S, Zacher W. 1981. The Wadi Shueib structure in Jordan. Neues Jahrbuch für Geologie und Paläontologie, Monatshefte, 9: 571–576.

Moore K B, Ekwurzel B, Esser B K, et al. 2006. Sources of groundwater nitrate revealed using residence time and isotope methods. Applied Geochemistry, 21(6): 1016–1029.

Nigro A, Sappa G, Barbieri M. 2017. Strontium isotope as tracers of groundwater contamination. Procedia Earth Planetary Science, 17: 352–355.

Nixon S W. 2009. Eutrophication and the macroscope. Hydrobiologia, 629: 5–19.

Nyam F M E A, Yomba A E Y, Tchikangoua A N, et al. 2020. Assessment and characterization of groundwater quality under domestic distribution using hydrochemical and multivariate statistical methods in Bafia, Cameroon. Groundwater for Sustainable Development, 10: 100347, doi: 10.1016/j.gsd.2020.100347.

Obeidat M M, Massadeh A M, Al-Ajlouni A M, et al. 2007. Analysis and evaluation of nitrate levels in groundwater at Al-Hashimiya area, Jordan. Environmental Monitoring and Assessment, 135: 475–486.

Obeidat M M, Awawdeh M, Al-Rub F A, et al. 2012. An innovative nitrate pollution index and multivariate statistical investigations of groundwater chemical quality of Umm Rijam Aquifer (B4), North Yarmouk River Basin, Jordan. In: Vouddouris K, Voutsa D. Water Quality Monitoring and Assessment. Croatia: InTech, 169–188.

Obeidat M M, Awawdeh M, Matiatos I, et al. 2020. Identification and apportionment of nitrate sources in the phreatic aquifers in Northern Jordan using a dual isotope method ($\delta^{15}N$ and $\delta^{18}O$ of NO_3^-). Groundwater for Sustainable Development, 100505, doi: 10.1016./j.gsd.2020.100505.

Panagopoulos G, Lambrakis N, Katagas C, et al. 2005. Water-rock interaction induced by contaminated groundwater in a karst aquifer, Greece. Environmental Geology, 49: 300–313.

Panno S, Kelly W, Martinsek A, et al. 2006. Estimating background and threshold nitrate concentrations using probability graphs. Ground Water, 44(5): 697–709.

Parkhurst D L, Appelo T. 1999. User's guide to PHREEQC (version 3): A computer program for speciation, batch-reaction, one-dimensional transport, and inverse geochemical calculations. Denver, Colorado: USGS (United States Geological Survey).

Parnell A C, Inger R, Bearhop S, et al. 2010. Source partitioning using stable isotopes: coping with too much variation. PLoS ONE, 5(3): e9672, doi: 10.1371/journal.pone.0009672.

Popescu R, Mimmo T, Dinca O R, et al. 2015. Using stable isotopes in tracing contaminant sources in an industrial area: A case study on the hydrological basin of the Olt River, Romania. Science of the Total Environment, 533: 17–23.

Powell J. 1989. Stratigraphy and sedimentation of the phanerozoic rocks in Central and South Jordan. Kurnub, Ajlun and Belqa Groups. Amman: The Natural Resources Authority Bulletin.

Qin R, Wu Y, Xu Z, et al. 2013. Assessing the impact of natural and anthropogenic activities on groundwater quality in coastal alluvial aquifers of the lower Liaohe River Plain, NE China. Applied Geochemistry, 31: 142–158.

Rashid A, Khttab S A, Alim L, et al. 2019. Geochemical profile and source identification of surface and groundwater pollution of District Chitral, Northern Pakistan. Microchemical Journal, 145: 1058–1065.

Re V, Sacchi E. 2017. Tackling the salinity-pollution nexus in coastal aquifers from arid regions using nitrate and boron isotopes. Environmental Science and Pollution Research, 24: 13247–13261.

Re V, Sacchi E, Kammoun S, et al. 2017. Integrated socio-hydrogeological approach to tackle nitrate contamination in groundwater resources: The case of Grombalia Basin (Tunisia). Science of the Total Environment, 593–594: 664–676.

Riepl D. 2013. Knowledge-based decision support for integrated water resources management with an application for Wadi Shueib, Jordan. PhD Dissertation. Karlsruhe: University of Karlsruhe.

Rubasinghe R, Mukherjee R, Chandrajith R. 2015. Geochemical characteristics of groundwater in different climatic zones of Sri Lanka. Environmental Earth Science, 74: 3067–3076.

Sawyer C N, McCarty P L. 1967. Chemistry for sanitary engineers (2nd ed.). New York: McGraw-Hill, 518.

Schoeller H. 1967. Qualitative evaluation of ground water resources. In: Schoeller, H. Methods and Techniques of Groundwater Investigation and Development, Water Resource Series No. 33. Paris: UNESCO, 44–52.

Selvam S, Venkatramanan S, Chung S Y, et al. 2016. Identification of groundwater contamination sources in Dindugal district of Tamil Nadu, India using GIS and multivariate statistical analyses. Arabian Journal of Geosciences, 9(5): 407, doi: 10.1007/s12517-016-2417-7.

Senarathne S L, Jayawardana J M C K, Edirisinghe E A N V, et al. 2019. Characterization of groundwater in Malala Oya river basin, Sri Lanka using geochemical and isotope signatures. Groundwater for Sustainable Development, 9: 100225, doi:10.1016/j.gsd.2019.100225.

Shalev N, Burg A, Gavrieli I, et al. 2015. Nitrate contamination sources in aquifers underlying cultivated fields in an arid region-The Arava Valley, Israel. Applied Geochemistry, 63: 322–323.

Soldatova E, Guseva N, Sun Z, et al. 2017. Sources and behaviour of nitrogen compounds in the shallow groundwater of agricultural areas (Poyang Lake basin, China). Journal Contaminant Hydrology, 202: 59–69.

Stuyfzand P J. 2008. Base exchange indices as indicators of salinization or freshening of (coastal) aquifers. In: 20th Salt Water Intrusion Meeting. Naples, Florida, USA.

Sui Y, Ou Y, Yan B, et al. 2020. A dual isotopic framework for identifying nitrate sources in surface runoff in a small agricultural watershed, Northeast China. Journal of Cleaner Production, 246: 119074, doi: 10.1016/j.jclepro.2019.119074.

Ta'any R. 1992. Hydrological and hydrochemical study of the major springs in Wadi Shu'eib catchment area. MSc Thesis. Jordan: Yarmouk University.

Tarawneh M S M, Janardhana M R, Ahmed M M. 2019. Hydrochemical processes and groundwater quality assessment in North eastern region of Jordan valley, Jordan. HydroResearch, 2: 129–145.

Tesoriero A J, Saad D A, Burow K R, et al. 2007. Linking ground-water age and chemistry data along flow paths: implications for trends and transformations of nitrate and pesticides. Journal of Contaminant Hydrology, 94(1–2): 139–155.

Thibodeau B, Hélie J F, Lehmann M F. 2013. Variations of the nitrate isotopic composition in the St. Lawrence River caused by seasonal changes in atmospheric nitrogen inputs. Biochemistry, 115(1–3): 287–298.

Thilakerathne A, Schuth C, Chandrajith R. 2015. The impact of hydrogeological settings on geochemical evolution of groundwater in karstified limestone aquifer basin in Northwest Sri Lanka. Environmental Earth Sciences, 73: 8061–8073.

Tiwari A K, Pisciotta A, De Maio M. 2019. Evaluation of groundwater salinization and pollution level on Favignana Island, Italy. Environmental Pollution, 249: 969–981.

Venkiteswaran J J, Boeckx P, Gooddy D C. 2019. Towards a global interpretation of dual nitrate isotopes in surface waters. Journal of Hydrology, 4: 100037, doi: 10.1016/j.hydroa.2019.100037.

Vitoria L, Soler A, Canals A, et al. 2008. Environmental isotopes (N, S, C, O, D) to determine natural attenuation processes in nitrate contaminated waters: Example of Osona (NE Spain). Applied Geochemistry, 23(12): 3597–3611.

Wakida T F, Lerner D N. 2005. Non-agricultural sources of groundwater nitrate: A review and case study. Water Research, 39(1): 3–16.

Werz H. 2006. The use of remote sensing imagery for groundwater risk intensity mapping in the Wadi Shueib, Jordan. PhD Dissertation. Karlsruhe: University of Karlsruhe.

WHO (World Health Organization). 2011. Guidelines for Drinking Water Quality (4th ed.). Geneva: WHO.

Widory D, Kloppmann W, Chery L, et al. 2004. Nitrate in groundwater: An isotopic multi-tracer approach. Journal of Contaminant Hydrology, 72(1–4): 165–188.

Widory D, Petelet-Giraud E, Brenot A, et al. 2013. Improving the management of nitrate pollution in water by the use of isotope monitoring: the $\delta^{15}N$, $\delta^{18}O$ and $\delta^{11}B$ triptych. Isotopes in Environmental and Health Studies, 49(1): 29–47.

WSPSP (Water Sector Planning Support Project). 2004. National Water Master Plan. Amman: Ministry of Water and Irrigation, and Bonn: German Technical Cooperation, 97.

Xia Y Q, Li Y F, Zhang X Y, et al. 2017. Nitrate source apportionment using a combined dual isotope, chemical and bacterial property, and Bayesian model approach in river systems. Journal of Geophysical Research: Biogeosciences, 122(1): 2–14.

Xue D, Botte J, De Baets B, et al. 2009. Present limitations and future prospects of stable isotope methods for nitrate source identification in surface- and groundwater. Water Research, 43(5): 1159–1170.

Yang X, Liu Q, Fu G, et al. 2016. Spatiotemporal patterns and source attribution of nitrogen load in a river basin with complex pollution sources. Water Research, 94: 187–199.

Yu L, Zheng T, Zhen X, et al. 2020. Nitrate source apportionment in groundwater using Bayesian isotope mixing model based on nitrogen isotope fractionation. Science of the Total Environment, 718: 137242, doi: 10.1016/j.scitotenv.2020.137242.

Zaidi F K, Nazzal Y, Jafri M K, et al. 2015. Reverse ion exchange as a major process controlling the groundwater chemistry in an arid environment: A case study from northwestern Saudi Arabia. Environmental Monitoring and Assessment, 187: 607, doi:

10.1007/s10661-015-4828-4.

Zemann M, Wol L, Grimmeise F, et al. 2015. Tracking changing X-ray contrast media application to an urban-influenced karst aquifer in the Wadi Shueib, Jordan. Environmental Pollution, 198: 133–143.

Zendehbad M, Cepuder P, Loiskandl W, et al. 2019. Source identification of nitrate contamination in the urban aquifer of Mashhad, Iran. Journal of Hydrology: Regional Studies, 25: 100618, doi: 10.1016/j.ejrh.2019.100618.

Zhang Q, Wang X, Sun F, et al. 2015. Assessment of temporal and spatial differences of source apportionment of nitrate in an urban river in China, using $\delta^{15}N$ and $\delta^{18}O$ values and an isotope mixing model. Environmental Science and Pollution Research, 22: 20226–20233.

Zhang Q, Wang H. 2020. Assessment of sources and transformation of nitrate in the alluvial-pluvial fan region of North China using a multi-isotope approach. Journal of Environmental Sciences, 89: 9–22.

Zhang Y, Shi P, Li F, et al. 2018. Quantification of nitrate sources and fates in rivers in an irrigated agricultural area using environmental isotopes and a Bayesian isotope mixing model. Chemosphere, 208: 493–501.

Zhao Y, Zheng B, Jia H, et al. 2019. Determination sources of nitrates into the Three Gorges Reservoir using nitrogen and oxygen isotopes. Science of the Total Environment, 687: 128–136.

Zhu G F, Su Y H, Huang C L, et al. 2010. Hydrogeochemical processes in the groundwater environment of Heihe River Basin, Northwest China. Environmental Earth Sciences, 60: 139–153.